Universidade de Aveiro Departamento de Física,
2020

João Pedro Dias Rodrigues

A Study of possibilities beyond the Standard Model

o júri / the jury

presidente	**Margarida Facão** Professora Auxiliar do Departamento de Física da Universidade de Aveiro
vogais	**António Morais** Investigador Pos-doc do Departamento de Física da Universidade de Aveiro
	Nuno Castro? Professor at the University of Minho. Researcher at LIP and ATLAS experiment at CERN.

agradecimentos / acknowledgements

Honestamente acho que isto vai ter que ser escrito antes da entrega,REMINDER agradecer ao Morais! Pedro Ferreira Roman e Ian, sem o trabalho deles estava perdido.

Honestly this will be written in english translated poorly from above :)

Resumo

É impossível debater que o surpreendente sucesso do modelo padrão de física de partículas o faz um dos maiores sucesso da ingenuidade humana, no entanto, apesar de o modelo padrão descrever com grande detalhe todas as partículas observadas e as suas interações e conseguir tratar um grande número de fenomeno físicos onde era esperado encontrar falhas, tudo numa estrutura bem motivada, este é considerado incompleto.
Introduzir motivação para a falha do SM.
Introduzir motivação para mais Higgs.
Introduzir motivação para o BLSM
Introduzir motivação para o 3HDM
Tocar nas conclusões??

Abstract This part will be in English. Translated from above.

Contents

List of Figures

List of Tables

0.4 Labels

A paragraph or text to be added later
A mistake or a question that is likely wrong
A comment or doubt to ask or check
Excess? Probably will cut, waiting for advice

Chapter 1

Introduction

Modern study of particle physics must be taught trough the Standard Model (SM) of particle physics. The SM has thus far the best descriptor for the experimentally observed spectra of particles and their interactions at all current probable scales. And In 2012 a resonance was discovered in the LHC that seems to confirm the existence of it's last predicted particle, the Higgs boson, finally completing the Model and proving the existence of the Higgs mechanism [2, 3, 4, 5].

The development of the SM was a arduous task, it led scientists successfully combine three of the four fundamental forces of nature in a very well motivated framework, making it one of the most monumental achievements in physics. However, despite it's successes the SM still lacks a strong theoretical explanation for several experimental observations. They have become more numerous by the decade, and to provide a "short" overview of some of them.

We firstly have the fact the SM can not account for one of the most important cosmological discoveries of the century, the existence of dark matter. This is a fundamental flaw since the SM lacks a possible dark matter candidate, or dark particle. Secondly, the SM lacks any justification for the existence of baryon asymmetry in the universe, i.e. why is the universe primarily made of matter rather than anti-matter. Although note that the Electroweak baryogenesis (EWBG) remains a theoretically possible scenario for explaining the cosmic baryon asymmetry, a scenario viable in the SM framework. Thirdly, the SM suffers from peculiar oddities in the fermion sector in the form of unjustified mass and mixing hierarchies. This is usually refereed to as the *flavour problem* and is considered a sizeable drawback of the SM. As a example, we observe the top quark to be five order of magnitudes heavier the up quark, and eleven orders of magnitude than the observed neutrino masses. These high differences are thought to be too large to be natural, so a physical property that would justify such gap is a desired property of most Beyond the Standard Model (BSM) frameworks. Fourth, note neutrino masses are not included in the SM. Although there are precise oscillation measurements that measure masses in the eV range with precise mixing in between 3 different generations of neutrinos. There are still many other subtitle flaws, like the lack of a strong phase transition, etc.

These are just some of the typical justifications given to explore possible BSM scenarios.

The holy grail of which would be a model that include all these problems in a properly motivated framework that addresses these and many more cosmological, gravitational, and phenomenological problems. For now such a model remains out of reach, so the narrowing down of theories through phenomenological studies is a very worthwhile endeavour. We try to present one of these studies in this work. Paradoxically fortunately, as of late these studies have become progressively harder to perform given that the available space for new physics gets reduced by each successful particle experiment. Chief among these experiments is the Large Hadron Collider (LHC), whose large amount of collect data over past years is setting more and more stringent bounds on viable parameter spaces of popular BSM scenarios. And as available space for new physics decreases it becomes more challenging to reveal remaining space without falling within the possibility of fine tuning our model.

Note, that the SM has shown increasingly consistence with most constraints that were initial believed to be a possible gateway to new physics (NP) or that would diverge from it's predictions. Thus, the search continues for hints at possible directions to complete the SM.

Conventionally, phenomenological simulations of BSM searches in these multi-dimensional parameter spaces have been made in large computer-clusters with use of several weeks of computational time trough simple Monte-Carlo methods. Although this is the basis of the work presented here a effort was made to incorporate new machine learning routines trough the initial building of smaller learning sets trough conventional methods. Unfortunately this wasn't accomplished in this work due to the expectational setbacks. A feature of this year, that affected partially the quality of the work.

During this work we shall do a small expedition into two possible BSM scenarios. To achieve this, we will start by laying down the fundamental basis for this BSM discussion by presenting a short overview of the SM, then we discuss possible extensions to the SM. Namely, first by presenting the B-L-SM model, a simple unitary extension based on a apparently accidental symmetry of the SM. And then by moving on to a more complex model with additional Higgs doublets fields as a attempt to present a framework that addresses the *flavour problem*. We will see how these multiple doublet Models can address problems that simple unitarity extension can't and vice-versa. For example multiple Higgs Doubles can easily offer a explanation for the observed excess of charge parity or $\mathcal{CP}$ violation. But suffer from the possible inclusion of tree-level Flavour Changing Neutral Currents (FCNCs). These FCNCs are undesirable at least in large number given observations, so mechanisms have to be put in place to prevent them, while in the case of the simple unitary extensions such problems do not arise.

I also want to stress that, while the minimally structure of the Higgs sector postulated by the SM is not a immediate contradiction of measurements. It is not manifestly required by the data. And in fact a extended scalar sector is often desired despite the relatively tight bounds on Higgs boson couplings to SM gauge boson and heavy fermions. These additions are motivated also in part by in the SM, the single Higgs doublet is a bit "overstretched". It takes care simultaneously of the masses of the gauge bosons and of the up and down-type fermions and leptons. N-Higgs-doublet models and scalar or complex fields, relax this requirement. In particular the multiple Higgs doublet models are based "natural", suggestion, that the notion of generations can be brought to the Higgs sector.

Chapter 2

The Standard Model of Particle Physics

2.1 Motivation

Has stated, it is hard to question the validity of the SM as a successful, at least approximate, framework with whom to describe the phenomenology of Particle Physics up to the largest energy scales probed by collider measurements so far, although some inconsistencies remain and must be addressed. The SM was proposed in the nineteen sixties by Glashow, Salam and Weinberg and since it has been extensively tested. Both in contemporary direct searches for new physics and indirect probes via e.g. flavour anomalies and precise electroweak parameter measurements in proton-electron collisions.

The path to the formulation of the SM came from previous principles relating to symmetries in nature, specifically symmetry in physical laws. In fact, much in modern physics can be attributed to Emmy Noether's work. She deduced, trough her first theorem, that if the action in a system is invariant under some group of transformations (symmetry), then there exist one or more conserved quantities (constants of motion) which are associated to these transformations.

Physicist took this idea and were led to the fundamental question behind the SM, is it possible that upon imposing to a given Lagrangian the invariance under a certain group of symmetries to reach a given form for it's the dynamics? These dynamics would be in our context, particle interactions. This train of thought first led to Quantum Electrodynamics (QED), then Quantum Chromodynamics (QCD) and finally the SM. We can quote Salam and Ward:

"Our basic postulate is that it should be possible to generate strong, weak and electromagnetic interaction terms (with all their correct symmetry properties and also with clues regarding their relative strengths) by making local gauge transformations on the kinetic energy terms in the free Lagrangian for all particles."

We are glossing over a lot of complexity here, and for the SM to be properly formulated additional concepts would be required. In the case of weak interactions, the presence of very heavy weak gauge bosons require the new concept of spontaneous breakdown of the gauge symmetry and the Higgs mechanism [6, 7, 8] . While the concept of asymptotic freedom played a crucial role to describe perturbatively the strong interaction at short distances [9, 10].

2.2 Internal symmetry of the Standard Model

The SM is a "standard" QFT gauge theory, that is to say, it is manifestly invariant under a set of field transformations. The SM gauge group, $\mathcal{G}_{SM}$, is seen in,

$$\mathcal{G}_{SM} = \mathrm{SU(3)_c} \times \mathrm{SU(2)_L} \times \mathrm{U(1)_Y} \quad . \tag{2.1}$$

Here we have, first, the $\mathrm{SU(3)_c}$ group corresponding to quantum chromodynamics (QCD), responsible for the strong force, this symmetry will remain unbroken by the electroweak VEV. Secondly, we have the $\mathrm{SU(2)_L} \times \mathrm{U(1)_Y}$ portion that will be broken by the Higgs mechanism into $\mathrm{U(1)_Q}$, the electromagnetic gauge symmetry. Each particle stems from a field that is charged in a particular manner on each of these groups, making the charge triplets we will come to later define. Given the invariance under the group in eq. 2.1, it is impossible have any field that is charged have a explicit mass term. This chapter will focus on how the mass of particles is generate trough the Higgs mechanism. And offer a brief discussion of flavour physics in the SM and how flavour changing currents can point to New Physics (NP).

Gauge Group numbers

The full set of quantum numbers in all the SMs fields are described in the tables 2.1 and 2.2, this is their color charge, weak isospin number and the hypercharge, written in that order as entries in each triplet.

Table 2.1: Gauge and Scalar fields dimensions in the SM

Fields	Spin 0 field	Spin 1 Field	$SU(3)_C \times SU(2)_L \times U(1)_Y$
Gluons	$\times$	g	(8,1,0)
A bosons	$\times$	A^i	(1,3,0)
B bosons	$\times$	B	(1,1,0)
Higgs field	$(\phi^{\pm}, \phi^0)$	$\times$	(1,2,1)

Table 2.2: Fermion field dimensions in the SM

Fields	Spin $\frac{1}{2}$ Field	$SU(3)_C \times SU(2)_L \times U(1)_Y$
Quarks (3 gen.)	$Q = (u_L, d_L)$	$(3, 2, \frac{1}{3})$
	u_R	$(3, 1, \frac{4}{3})$
	d_R	$(3, 1, -\frac{2}{3})$
Leptons (3 gen.)	$(L = (\nu_{e_L}, e_L)$	$(1, 2, -1)$
	e_R	$(1, 1, -2)$

From here, given the gauge group in, eq. 2.1 and accounting for the charges and fields, we can derive the form of the SM's Lagrangian. These gauge groups are composed of 12 generators and are governed by the following algebra,

$$[L_a, L_b] = i f_{abc} L_c \quad [T_a, T_b] = 1 \epsilon_{abc} T_c \quad [L_a, T_b] = [L_a, Y] = [T_b, Y] = 0 \tag{2.2}$$

where for the $\mathrm{SU(3)_c}$ triplets, $L_a = \frac{\lambda_a}{2}$, $(a = 1, ..., 8)$ contrary to $\mathrm{SU(3)_c}$ singlets where, $L_a = 0$. As for the $\mathrm{SU(2)_L}$, we have $T_i = \frac{\sigma_i}{2}$, $(i = 1, 2, 3)$, being that again for singlets $T_b = 0$. Y is the generator of $U(1)_Y$. The symbols λ_a and σ_i represent the Gell-Mann and Pauli matrices respectively.

2.2.1 Fields, Particles and Lagrangian of the SM

From these fields the physical states of the SM, it's particle spectrum, is composed by, first, the gauge bosons, the weak force carriers, $W^{\pm}$ and Z bosons, and the photon γ, the electromagnetic interaction messenger and the strong force mediators, the gluons, g, as well, of course, by the matter particles, the fermions, composed by the quarks and leptons.

Leptons and quarks are organized in three generations each, with 2 pairs by each generation leading to 6 different particles for each. For quarks we have the up and down for the first generation, charm and strange for the second as well as top and bottom for the third one. Similarly, there are 6 types of leptons, the charged ones, electron, muon and tau, and the associated neutrinos. These are represented in different manners, being that the quarks are represented by the letters (u, d, c, s, t, b) while leptons as $(e, \nu_e, \mu, \nu_\mu, \tau, \nu_\tau)$.

Fermions are half integer spin particles half of which have electrical charge (except the neutrinos). While quarks interact via the weak, electromagnetic and strong forces, the charged leptons only feel the electromagnetic and weak forces and the neutrinos are weakly interacting. A physical fermion is composed of a left-handed and a right-handed field. While the left transform as $SU(2)_L$ doublets and can be written as,

$$L^i = \begin{pmatrix} \nu_{e_L} \\ e_L \end{pmatrix}, \begin{pmatrix} \nu_{\mu_L} \\ \mu_L \end{pmatrix}, \begin{pmatrix} \nu_{\tau_L} \\ \tau_L \end{pmatrix} \quad \text{and} \quad Q^i = \begin{pmatrix} u_L \\ d_L \end{pmatrix}, \begin{pmatrix} c_L \\ s_L \end{pmatrix}, \begin{pmatrix} t_L \\ b_L \end{pmatrix} \quad , \tag{2.3}$$

where the i index stands for generation, often designed as the flavour index, the latter are $\mathrm{SU(2)_L}$ singlets and can be simply represented as

$$e_R^i = \{e_R, \mu_R, \tau_R\}, \quad u_R^i = \{u_R, c_R, t_R\}, \quad d_R^i = \{d_{e_R}, s_{e_R}, b_{e_R}\} \quad , \tag{2.4}$$

note also that the quarks form triplets of $SU(3)_C$ whereas leptons are colour singlets. The Higgs boson also emerges from an $SU(2)_L$ doublet with the form,

$$H = \begin{pmatrix} \phi^1 + \ i\ \phi^2 \\ \phi^3 + \ i\ \phi^4 \end{pmatrix} \quad , \tag{2.5}$$

Here we see the four components that correspond to the respective degrees of freedom of the Higgs Field. After the process of SSB of the $SU(2)_L \times U(1)_Y$ group the charges of the fermions along their QCD and QED numbers become,

Table 2.3: Quark and Lepton charges

	$SU(3)_C$	$U(1)_Q$
Up type quarks (u, c, t)	3	2/3
Down type quarks (d, s, b)	3	-1/3
Charged leptons (e, μ, τ)	1	-1
Neutrinos $(\nu_e, \nu_\mu, \nu_\tau)$	1	0

Lagrangian formulation

Given the SM gauge groups and charges seen in 2.1 the covariant derivative, D_μ, will read as,

$$D_\mu = \partial_\mu - ig_S \tau^a G^a_\mu - igT^i A^i_\mu - ig' Y B_\mu \quad , \tag{2.6}$$

We can expect 3 different type of couplings, g_s related to the $SU(3)_C$ subgroup, g to the $SU(2)_L$ and g' to $U(3)_Y$. The associated canonical field strength tensors would be,

$$G^{\mu\nu}_a = \partial^\mu G^\nu_a - \partial G^\mu_a - g_s f_{abc} G^\mu_a G^\nu_b \tag{2.7}$$
$$A^{\mu\nu}_a = \partial^\mu A^\nu_a - \partial^\nu A^\mu_a - g \epsilon_{abc} A^\mu_b A^\nu_c \tag{2.8}$$
$$B^{\mu\nu} = \partial^\mu B^\nu - \partial^\nu B^\mu \tag{2.9}$$

It is often convenient to present the SMs Lagrangian in portions, usually divided in three sections,

$$\mathcal{L}_{SM} = \mathcal{L}_{kin} + \mathcal{L}_{Yuk} + \mathcal{L}_\phi \tag{2.10}$$

Where we have the kinetic portion of the SM terms,$\mathcal{L}_{kin}$, responsible for free propagation of particles, the Yukawa portion, $\mathcal{L}_{Yuk}$ corresponding to interactions of particles with the Higgs Boson, and finally the $\mathcal{L}_\phi$ scalar potential. The full kinetic portion of the SM read,

$$\begin{aligned} \mathcal{L}_{kin} = & - \frac{1}{4} G^{\nu\mu}_a G_{a\,\nu\mu} - \frac{1}{4} A^{\nu\mu}_a A_{a\,\nu\mu} - \frac{1}{4} B^{\nu\mu} B_{\nu\mu} \\ & - i\overline{Q_{L_i}} \not{D} Q_{L_i} - i\overline{u_{R_i}} \not{D} u_{R_i} - i\overline{d_{R_i}} \not{D} d_{R_i} - i\overline{L_{L_i}} \not{D} L_{L_i} - i\overline{e_{R_i}} \not{D} e_{R_i} \\ & - (D_\mu H)^\dagger (D^\mu H) \end{aligned} \tag{2.11}$$

Where $\not{D}$ is the Dirac covariant derivative, $\gamma^\mu D_\mu$. From the last line Eq. 2.11 and with Eq. 2.6 we will present how the Generators A^i_μ and B_μ give rise to the weakly interacting vector bosons $W^\pm$ and Z^0 and the electromagnetic vector boson γ. Contrary to the color sector, where the eight generators G^a_μ simply correspond to eight gluons g a mediating strong interactions. While the scalar potential part

$$\mathcal{L}_\phi = -\mu^2 HH^\dagger - \lambda(HH^\dagger)^2 \tag{2.12}$$

Finally the Yukawa portion of the Lagrangian would be written as,

$$\mathcal{L}_{Yuk} = Y^u_{ij}\overline{Q_{L_i}}u_{R_j}\tilde{H} + Y^d_{ij}\overline{Q_{L_i}}d_{R_j}H + Y^e_i j\overline{L_{L_i}}e_{R_i}H + h.c. \tag{2.13}$$

Here we have, $\tilde{H} = i\sigma_2 H$. We'll define these fields in the relevant section. Note that naturally all indices seem in Eqs. 2.11 2.12 and 2.13, (j, i) are summed over.

2.3 The Higgs mechanism and the mass generation of the Gauge bosons

From what was defined above, we can now study the process SSB by which,

$$\mathrm{SU(2)_L \times U(1)_Y \to U(1)_Q} \tag{2.14}$$

and carry trough to the Higgs Mechanism. Enabling us to find the real physical states of the gauge bosons and the origin of their mass. Let us then consider the part of the Lagrangian containing the scalar covariant derivatives, the scalar potential and the gauge-kinetic terms:

$$\mathcal{L}_{Gauge} \supset (D_\mu H)(D^\mu H)^\dagger - \mu^2 H^\dagger H - \lambda(H^\dagger H)^2 - \frac{1}{4}W^{\nu\mu}_a W_{a\,\nu\mu} - \frac{1}{4}B^{\nu\mu}B_{\nu\mu} \tag{2.15}$$

We expect a phase shift to occur, namely one that ensures $\mu^2 < 0$ while at the same ensuring that the field now explicitly breaks the $\mathrm{SU(2)_L \times U(1)_Y}$. For this to happen we expect the shifted squared value of the Higgs field to be,

$$(H^\dagger H) = \frac{-\mu^2}{2\lambda} = \frac{1}{2}v \quad , \tag{2.16}$$

This VEV, called the electroweak VEV, is experimentally measured to be $v \approx 246$ GeV. The choice of vacuum can be aligned in such a way that we have,

$$H_{min} = \frac{1}{\sqrt{2}}\begin{pmatrix} 0 \\ v \end{pmatrix} \quad . \tag{2.17}$$

Given that now the $SU(2)_L \times U(1)_Y$ symmetry is broken down to $U(1)_Q$ we jump from a scenario where there were four generators, which are $T^{1,2,3}$ and Y, to, after the breaking, having solely one unbroken combination that is $Q = (T^3 + 1/2)$ associated to the electric charge. This means that in total we will have three broken generators, thus, from Goldstone Theorem, there would have to be created three massless particles.

These Goldstones modes however can then be parametrized as phases in the field space and then can be "rotated away" in the physical basis, leaving us with a single physical massive scalar, the Higgs boson. Note that, with this transformation we are removing three scalar degrees of freedom. However, they cannot just disappear from the theory and will be absorbed by the massive gauge bosons. In fact, a massless gauge boson contains only two scalar degrees of freedom (transverse and polarization). Meanwhile, a massive vector boson has two transverse and a longitudinal polarization, i.e., three scalar degrees of freedom. So, as we discussed above, while before the breaking of the EW symmetry we have four massless gauge bosons, after the breaking we are left with three massive ones. This means that there are three extra scalar degrees of freedom showing up in the gauge sector. It is then commonly said that the goldstone bosons are "eaten" by the massive gauge bosons and the total number of scalar degrees of freedom in the theory is preserved. Therefore, without loss of generality, we can rewrite the Higgs doublet as

$$\begin{pmatrix} G_1 + iG_2 \\ v + h(x) + iG_3 \end{pmatrix} = H(x) \to H(x) = \frac{1}{\sqrt{2}} \begin{pmatrix} 0 \\ v + h(x) \end{pmatrix} \quad . \tag{2.18}$$

Once the Higgs doublet acquires a VEV, the Lagrangian (2.15) can be recast as:

$$\begin{aligned} \mathcal{L}' =& \frac{1}{2}\partial_\mu h \partial^\mu h - \frac{1}{2}(2v^2\lambda)h^2 - \frac{1}{4}W_a^{\nu\mu}W_{a\,\nu\mu} - \frac{1}{4}B^{\nu\mu}B_{\nu\mu} \\ &+ \frac{1}{8}v^2 g^2 (A^1_\mu A^{1,\mu} + A^2_\mu A^{2,\mu}) + \frac{1}{8}v^2(g^2 A^3_\mu A^{3,\mu} + g'^2 B_\mu B^\mu - 2g^2 g'^2 A^3_\mu B^\mu) \quad , \end{aligned} \tag{2.19}$$

A few things become obvious first, we have a lot of mass terms most stemming from the squared gauge fields and a lonesome squared mass term belonging to the real scalar field we know to be the Higgs field. This makes the Higgs boson mass in the SM to be given by,

$$M_h = (2v^2\lambda) \quad . \tag{2.20}$$

To obtain masses for the gauge bosons we need to rotate the gauge fields to a basis where the mass terms are diagonal. First, it is straightforward to see that the electrically charged eigenstates are given by

$$W^\pm_\mu = \frac{1}{\sqrt{2}}(A^{(1)}_\mu \pm iA^{(2)}_\mu) \quad , \tag{2.21}$$

meaning that the mass of the W bosons is,

$$M_{W^\pm} = \frac{1}{2}vg \quad . \tag{2.22}$$

The situation becomes a bit more complicated for the second term in (2.19) due to a mixing between A^3_μ and B_μ. In the gauge eigenbasis the mass terms read

$$\begin{pmatrix} A^3_\mu & B_\mu \end{pmatrix} \cdot \frac{1}{4}\nu^2 \begin{pmatrix} g^2 & -gg' \\ -gg' & g'^2 \end{pmatrix} \cdot \begin{pmatrix} A^3_\mu \\ B_\mu \end{pmatrix} \quad , \tag{2.23}$$

which can be diagonalized to obtain,

$$\begin{pmatrix} A_\mu & Z_\mu \end{pmatrix} \begin{pmatrix} 0 & 0 \\ 0 & \frac{1}{2}v\sqrt{g^2+g'^2} \end{pmatrix} \begin{pmatrix} A^\mu \\ Z^\mu \end{pmatrix} \quad , \tag{2.24}$$

we identify the eigenvector associated to the eigenvalue 0 to the photon and the massive one, $M_Z = \frac{1}{2}v\sqrt{g^2+g'^2}$, to the Z boson. Such eigenvectors can be written as

$$A_\mu = \cos(\theta_\omega)B_\mu + \sin(\theta_\omega)A^3_\mu \quad , \tag{2.25}$$

$$Z_\mu = -\sin(\theta_\omega)B_\mu + \cos(\theta_\omega)A^3_\mu \quad , \tag{2.26}$$

where θ_w is the so called Weinberg mixing angle and is defined as,

$$\cos(\theta_\omega) = \frac{g}{\sqrt{g^2+g'^2}} \quad , \tag{2.27}$$

thus clearly showing the massless photon along with a massive Z boson with mass $M_Z = \frac{1}{2}\nu\sqrt{g^2+g'^2}$. So we conclude our exploration of the electroweak sector with all the correct massive spectrum observed and its origin discussed.

2.4 Fermion Masses in the SM and Quark mixing

As referenced, given the charges of the fermion and lepton fields we cannot construct a gauge invariant theory with explicit mass terms for fermions. The mass of these particles are generated through couplings to the Higgs, by the Higgs mechanism. We can write these interactions as,

$$\mathcal{L}_{Yuk} = Y^u_{ij}\overline{Q_{L_i}}u_{R_j}\tilde{H} + Y^d_{ij}\overline{Q_{L_i}}d_{R_j}H + Y^e_i j\overline{L_{L_i}}e_{R_i}H + h.c. \tag{2.28}$$

where $Y^{e,u,d}$ stand for the Yukawa matrices, these are generic 3×3 complex non-dimensional coupling matrices, H is the Higgs field with $\tilde{H}$ retaining it's previous definition, i, j are the standard generation indices, Q_{L_i},are the left handed quark doublets, while d_R and u_R are the corresponding right-handed down and up quark singlets respectively in the weak eigenstate basis. Has the Higgs field settles into the electroweak VEV Eq. 2.28 yields mass terms for the quarks and leptons. The Higgs mechanism generates the mass for all the fermionic and leptonic particles except for neutrinos, this is due to the SM not containing right handed neutrinos, i.e we can't build terms that would lead to neutrino masses. The addition of right handed neutrino fields is very commonly made in BSM scenarios.

To reach the physical states starting from the weak eigenbasis you must diagonalize the Yukawa matrices. This is done through a bi-unitary transformation. We can write these transformation under the form,

$$M^{u,d,e}_{\text{diag.}} = U^{u,d,e}_L Y^{u,d,e} U^{u,d,e}_R \frac{v}{\sqrt{2}} \tag{2.29}$$

where v stands for the electroweak VEV. And $U_L^{u,d,e}$ and $U_R^{u,d,e}$ are the required 6 unitary matrices. It is, in fact, these matrices that will get us from the flavour eigenbase to the mass eigenbase. Naturally we can invert Eq. 2.29, returning equations for the Yukawa matrices as,

$$\begin{aligned} Y_{ij}^u &= \frac{\sqrt{2}}{v}(U_L^u M_{\text{diag.}}^u U_R^u)_{ij} \\ Y_{ij}^d &= \frac{\sqrt{2}}{v}(U_L^d M_{\text{diag.}}^d U_R^d)_{ij} \end{aligned} \tag{2.30}$$

We can see this change creates mass terms for physical quark fields by replacing the result of eq. 2.30 in the Yukawa portion of the Lagrangian (Eq. 2.13).

$$\begin{gathered} \mathcal{L}_{Yuk} \supset -\frac{v}{\sqrt{2}} Y_{ij}^d \begin{pmatrix} \overline{u}_{L\,i} & \overline{d}_{L\,i} \end{pmatrix} d_{R\,j} - \frac{v}{\sqrt{2}} Y_{ij}^u \begin{pmatrix} \overline{u}_{L\,i} & \overline{d}_{L\,i} \end{pmatrix} u_{R\,j} + h.c. \\ \Downarrow \\ -(U_L^d m_{\text{diag.}}^d U_R^d)_{ij} d_{L\,i}\, d_{R\,j} - (U_L^u m_{\text{diag.}}^u U_R^u)_{ij} u_{L\,i}\, u_{R\,j} + (\text{Interactions}) + h.c \\ \Downarrow \\ -m_{\text{diag.}_j}^d d'_{L\,i}\, d'_{R\,j} - m_{\text{diag.}_j}^u u'_{L\,i}\, u'_{R\,j} + (\text{Interactions}) + h.c \end{gathered} \tag{2.31}$$

where the primed fields are the quark fields in the mass basis, defined as,

$$\begin{aligned} d'_{L,R} &= U_{L,R}^d d_{L,R} \\ u'_{L,R} &= U_{L,R}^u u_{L,R} \end{aligned} \tag{2.32}$$

Note that the increasing masses seen in each generation depend directly on the term hierarchy of the Yukawa terms. This means that the mass of all particles directly relate to how strongly they each interact with the Higgs boson. If you then take into account the real masses e.g. for the leptons, the tau mass is in the GeV range while the electron's is in the 0.1 MeV range. These translate to very different couplings for each flavour. This hierarchy is unjustified in the SM.

As a result of this redefinition we can now look at the gauge interactions to see that a charge current appears where $W^{\pm}$ couples the physical u'_{L_j} and d'_{L_j}. The coupling of the of fermions to their respective gauge fields changes by virtue of the fact only left handed Quarks are $SU(2)_L$ doublets, if we expand the up and down quark fields on the kinetic portion of the Lagrangian,

$$\begin{aligned} \mathcal{L}_{ferm} \supset & \frac{1}{2}\overline{u'_L}\gamma^\mu \left(g' Y_L B_\mu + g W_\mu^0\right) \left(U_L^u U_L^{u\dagger}\right) u'_L - \frac{1}{\sqrt{2}} g \overline{u'_L}\gamma^\mu \left(U_L^u U_L^{d\dagger}\right) d'_L W_\mu^+ \\ & - \frac{1}{\sqrt{2}} g d'_L \gamma^\mu \left(U_L^u U_L^{d\dagger}\right) u'_L W_\mu^- + \frac{1}{2}\overline{d'_L}\gamma^\mu \left(g' Y_L B_\mu - g W_\mu^0\right) \left(U_L^d U_L^{d\dagger}\right) d'_L \end{aligned}$$

We can trough the use of the properties of unitary matrices, namely, $\mathrm{U}_{L,R}^{u,d}\mathrm{U}_{L,R}^{u,d\dagger} = 1$, note that the interactions with the neutral bosons remain the same in the mass basis.

However the charged currents are affected by this change. There for, we define the Cabibbo-Kobayashi-Maskawa (CKM) matrix, as $V_{CKM} = U_L^u U_R^{u\dagger}$ and write the sensitive terms,

$$\mathcal{L}_{kin} \supset \frac{1}{\sqrt{2}} g \overline{u}'_L \gamma^\mu V_{CKM} d'_L W_\mu^+ + h.c. \tag{2.33}$$

The CKM matrix, is a 3×3 unitary matrix. It is a parametrization of the three mixing angles and CP-violating KM phase. There are many possible conventions to represent the CKM matrix. The mixing angles refer to those between the up and down quark families. We can see their hierarchy in Fig. 2.2.

It is through this complex phase in the CKM matrix that the SM can account for the phenomena of $\mathcal{CP}$ violation. First observed in the famous K^0 decay into μ^+ μ^- ($CP = +1$ and $CP = -1$ respectively) that won the 1980 Nobel Prize. The discovery opened the door to questions still at the core of particle physics and of cosmology today. Not just the lack of an exact CP-symmetry, but also the fact that it is so close to a symmetry. citation

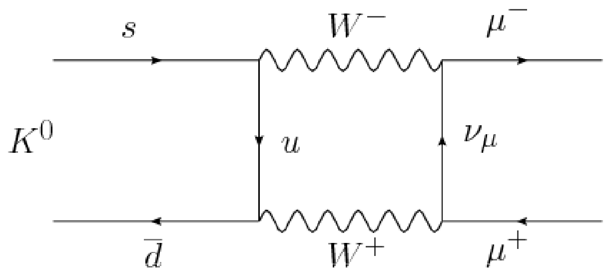

Figure 2.1: Box diagram describing $K_L^0 \to \mu^- \mu^+$, through an intermediate u quark.

We avoided discussing leptons since in the SM their mass eigenstates can be easily shown to have no real consequence besides a change of basis. You might also note a very interesting feature of the Standard Model, by consequence of the $\mathrm{SU(2)_L} \times \mathrm{U(1)_Y}$ symmetry there are no interactions of the right handed unitary matrices and there for no mixing, coupling, or charged currents of right handed quarks, making them theoretically invisible to measurements.

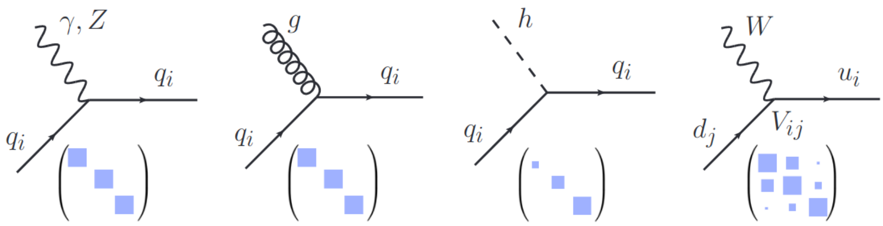

Figure 2.2: The Feynman diagrams for flavour conserving couplings of quarks to photon, Z boson, gluon and the Higgs (the first three diagrams), and the flavour changing coupling to the W (the last diagram). The 3×3 matrices are visual representations of couplings in the generation space, with couplings to γ ,Z, g flavour universal, the couplings to the Higgs flavour diagonal but not universal, and the couplings to W flavour changing and hierarchical.

The CKM matrix elements are fundamental parameters of the particle physics, so their precise determination is important, and reproducing the quark mixing parameters is fundamental for BSM searches that include changes to how the quarks interact with possible new Higgs bosons.

2.4.1 Charged Flavour Currents vs. Neutral Flavour Currents

In the SM there is a very important distinction between flavour changing neutral and charged currents. Flavour Changing Neutral Currents (FCNCs) are processes in which the quark flavour changes, while the quark charge stays the same. The Flavour Changing Charged Currents (FCCCs) change both the flavour and the charge of the quark. Extracting some representative probabilities from [11] reveals that the two types of processes are strikingly different. The charged currents lead to the dominant weak decays, while the FCNC induced decays are extremely suppressed. Rounding the experimental results, and not showing the errors, a few representative decays are,

Table 2.4: FCCCs examples

$s \to u\mu^- \nu_\mu$	: Br $(K^+ \to \mu^- \nu) = 64\%$
$b \to cl^- \nu_l$	: Br $(B^- \to D^0 l \overline{\nu}_l) = 2.3\%$
$c \to u\mu^- \nu_\mu$	: Br $(D^\pm \to K^0 \mu^\pm \nu) = 9\%$

Table 2.5: FCNCs examples

$s \to d\mu^+ \mu^-$	: Br $(K_L \to \mu^+ \mu^-) = 7 \times 10^{-9}$
$b \to d\mu^+ \mu^-$	: Br $(B^- \to K^{*-} l^+ l^-) = 5 \times 10^{-7}$
$c \to ul^+ l^-$	: Br $(D^0 \to \pi l^+ l^-) = 1.8 \times 10^{-4}$

The reason for such a striking difference is that in the SM the charged currents occur at tree level, while FCNCs are forbidden at tree level and only arise starting at one loop order, note the lack of neutral couplings between the up and down families in Eq **??**. The relative complexity of these processes can be easily seen in Fig 2.3,

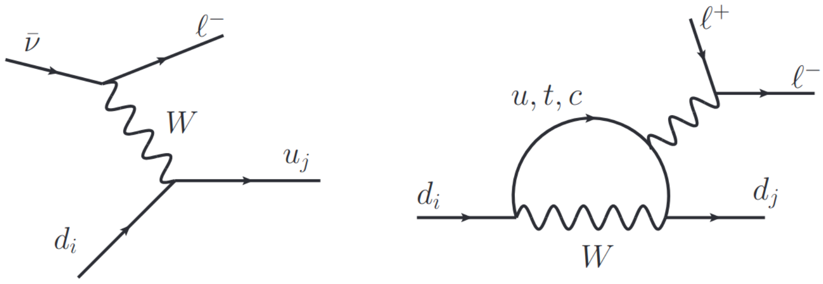

Figure 2.3: Representative tree level charged current diagram (left) and a loop induced FCNC diagram (right).

Furthermore, the FCNCs come suppressed by the difference of the masses of the quarks running in the loop, $m_j^2 - m_i^2$. This so called Glashow-Iliopoulos-Maiani (GIM) mechanism [12]. Given the diferences between the masses of the up and down sectors it has a significant impact. A interesting result of this mechanism would be that that there is no flavour violation, if all the quark masses are the same.

Flavour as a Probe into New Physics

Now that we have introduced without great detail flavour physics we can briefly touch on why collider experiments have been sold a as a pathway to discovering new physics i.e. how deviation in rare decays could pin point exactly what is missing in the Standard Model.

Thanks to these large experiments we have many new observables in flavour physics, e.g. the branching ratios, asymmetries, distributions. For each of these examples there is also a plethora of different parent particles for each change of flavour, as well as many instances of final states. The abundance of observables is clearly illustrated by opening the handy Particle Data Group (PDG) book [11] where even the condensed version, the PDG booklet, clocks out at more than 170 pages of mostly tabled information about these observables.

The recipe then, seems simple, identify processes that are rare in the SM and then search for deviations from the SM predictions. However thus far all but two processes are within 2σ experimental and theoretical bounds given by the SM. These are the $b \to s\mu\mu$ and $b \to c\tau\nu$ channels. They are, so far, showing over 4σ deviations from the their expected value. (citation needed). Without going into too much depth onto the NP searches, we can examine the scale at which these processes are "integrated away". This is the energy scale at which a NP vector-axial operator would allow these processes to exist only at high energies. These energies are naturally high given the terms in 2.34.

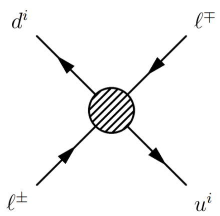

$$\mathcal{L}_{NP} \supset \frac{1}{\Lambda_{NP}} (\overline{Q}_i \gamma^\mu \sigma^A Q_j)(\overline{L}_k \gamma_\mu \sigma^A L_l) \tag{2.34}$$

Figure 2.4: "Contact" interactions with loop interactions containing NP

To explain $b \to s\mu\mu$ transitions you would need a $\Lambda_{NP} \approx 3$ TeV while for $b \to c\tau\nu$ you would need a $\Lambda_{NP} \approx 30$ TeV. This is a strong indicator that some components are missing in our formulation like a new mediator for gauge interactions. And the advantage of this scale is it almost certainly in most BSM scenarios, avoiding most experimental constraints.

As for the FCNC diagram for the $b \to s\mu\mu$ channel can be seen in Fig 2.5,

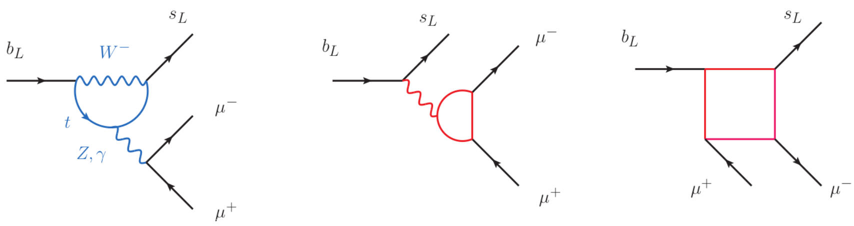

Figure 2.5: A representative SM diagram for $b \to s\mu\mu$ transition (left), and representative possible loop level NP contributions (middle and right).

The $b \to c\tau\nu$ flavour anomaly is similarly very clean theoretically [13]. However, the NP effect in these diagrams is large (citation needed) and often this means that the scale of NP needs to be lower than in the previous case. Consequently the NP interpretations here are often in conflict with experimental constraints (citation needed). This means the most obvious candidates are ruled out. Theoretical bias would have been that the new charged currents are either due to a charged Higgs, H^+ , or a new vector boson, W', see Fig. 2.6 (citation needed).

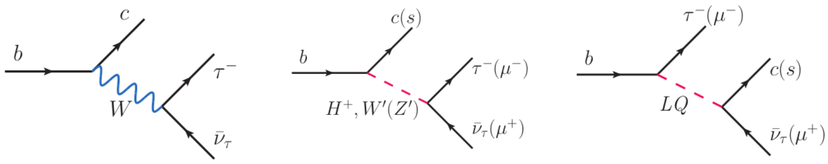

Figure 2.6: The SM diagrams for $b \to c\tau\nu$ transition (left), and the possible tree level NP contributions to $b \to c\tau\nu$ transition (middle and right).

Another prediction of the SM is that the rates for the $b \to se^+e^-$ and $b \to s\mu^-\mu^+$ transitions should be equal to each other. The SM prediction of Lepton Flavour Universality (LFU) is deeply engrained in the structure of the theory, since it is a consequence of the fact that the electroweak gauge group is the same for all three generations. The prediction of LFU can be tested experimentally, also trough flavour physics, by theoretically clean observables such as the ratios of these flavour observables,

$$R_{K^*} = \frac{\text{Br}(B \to K^*\mu^-\mu^+)}{\text{Br}(B \to K^*e^-e^+)} \tag{2.35}$$

Another strong indicator of new physics is the fact the experimental value for this ratio is $R_{K^*} \approx 0.7$, violating LFU by $2.2 - 2.6\sigma$ (citation needed).

The Future of Flavour Indirect Searches

The NP searches with rare decays, as well boost with the upcoming Belle II and LHC upgrades. Belle II expects to collect 50 times the Belle dataset. First collisions were seen in May 2018, and the first B physics run is expected in March 2019. While for the LHC, after upgrade II aims for roughly 100 times the present data set with an upgraded detector. (citation needed). Undoubtedly this improvement in sensibility will translate to a finer value for all measurable parameters at these experiments. We expect these anomalies then to go over the required 5σ in future experiments (Assuming of course, they are not statistical deviations). (citation needed).

Chapter 3

B-L-SM Model

Here we start the our first look at BSM scenarios. In this chapter we introduce the minimal $U(1)_{B-L}$ gauge extension of the Standard Model named, the B-L-SM Model [14, 15, 16]. This is a model trough which we can explain neutrino mass generation via a simple see-saw mechanism, additionally, by virtue of the model containing two new physical particle states, specifically a new Higgs like boson H' and a Z' gauge Boson we can also address other phenomenology, such as deviations in electro-weak measurements, namely the $(g-2)_\mu$ anomaly. The discrepancy between the measured anomalous magnetic moment of the muon and the SM expected value [17].

Both the additional bosons are given mass primarily trough the spontaneous breaking of the $U(1)_{B-L}$ symmetry that gives it's name to the Model. This unitary group originates from the promotion of a accidental symmetry present in the SM, the Baryon number (B) minus the Lepton number (L) to a fundamental Abelian symmetry group. This origin for the mass of the referenced bosons means model is already very heavily constricted due to long-standing direct searches in the Large Hadron Collide (LHC).

Trough this model we can address the metastability of the electroweak (EW) vacuum in the SM trough the new scalar. Allowing for Higgs stabilization up to the plank scale with a the new Higgs starting from few hundred of GeVs [18, 19, 20].

The B-L-SM is particular interesting in the context of the study of Grand Unified Theories (GUT) as it easily embedded into higher order symmetry groups like for example the SO(10) [21, 22, 23, 24, 25] or E_6 [26, 27, 28].

The presence of a new complex singlet field, χ, with a (tradicional) Higgs doublet typically results in enhanced strength of the EW phase transition potentially converting it into a strong first-order one, this would be could be detectable in the form of a gravitational wave background [29]. Such a analysis is of utmost importance given that it could provide a way to detect NP or exclude models without the need for a larger particle collider but instead a sensitive probe also capable of studying gravitational events.

However a family-universal symmetry such as $U(1)_{B-L}$ being introduced without changing the SM fermion content would lead to chiral anomalies. This translates to a non conservative charged current on some channels involving the $U(1)_{B-L}$. These aren't completely undesired by themselves, since their result would be charge conjugation parity symmetry violation, but this inclusion at tree-level without a suppression mechanism would lead to far too much $\mathcal{CP}$ violation.

The model also benefits from presence of three generations of right-handed heavy Majorana neutrinos that trough the new field additions are possible in a framework free of anomalies while also enabling a minimal see-saw mechanism to generate light neutrino masses unlike the SM. [30, 31, 32].´ The mass scale of such neutrinos is established once the $\mathrm{U(1)_{B-L}}$ symmetry is broken. These neutrinos are of cosmological significance given their presence could imply the existence of a sterile state that can play the role of Dark Matter candidate [33]. The relatively small alteration of a, $\mathbb{Z}_2$, symmetry in the neutrino sector can make these fully sterile, as seen in [34, 35]. Check if the Z2 affects the Zprime, if so we must comment that it doens't allow kinetic mixing! and would alter the a_μ These neutrinos can, in such case, be used to help explain the baryon asymmetry via the leptogenesis mechanism, this scenario is discussed in depth in the following Refs. [36, 37, 38].

The structure of this chapter is to first present the fundamental theoretical background on the model with a strong focus on the basic details of scalar and gauge boson mass spectra and mixing. Followed by a modern precise study of the phenomenological status of the B-L-SM model trough a layered algorithm that will be discussed preceding the results. Through this algorithm we provide a numerical analysis that tests the relevant phenomenological constraints in direct and electroweak observables. Followed by this study we table of a few representative benchmark points to be possibly tested in by experiments.

perhaps I should include this on the start of the chapter

3.1 Formulating the model

Essentially, the minimal B-L-SM is a BSM framework containing only three new ingredients, a new gauge interaction given the new symmetry group, three generations of right handed neutrinos, and a complex scalar field χ.

The first of these, is motivated by the aforementioned GUT scenarios, as seen in the Refs, [21, 22, 23, 24, 25, 26, 27, 28].

Secondly, as mentioned, a new sector of additional three $U(1)_{B-L}$ charged Majorana neutrinos is essential for anomaly cancellation and addresses many concerns of the SM.

Finally, the SM-like Higgs doublet, H, does not carry neither baryon nor lepton number, this way it does not participate in the breaking of $U(1)_{B-L}$. It is then necessary to introduce a new scalar singlet field, χ, solely charged under $U(1)_{B-L}$, to perform the breaking of the $B-L$ symmetry.

The particle content and related charges of the minimal $U(1)_{B-L}$ extension of the SM are shown in the table. Note these are similar to the SM as to be expected.

	q_L	u_R	d_R	l_L	e_R	ν_R	H	χ
$SU(3)_c$	3	3	3	1	1	1	1	1
$SU(2)_L$	2	1	1	2	1	1	2	1
$U(1)_Y$	$\frac{1}{6}$	$\frac{2}{3}$	-$\frac{1}{3}$	-$\frac{1}{2}$	-1	0	$\frac{1}{2}$	0
$U(1)_{B-L}$	$\frac{1}{3}$	$\frac{1}{3}$	$\frac{1}{3}$	-1	-1	-1	0	2

Table 3.1: Quantum fields and their respective quantum numbers in the minimal B-L-SM extension. The last two lines represent the weak and $B-L$ hypercharges

Scalar sector

Given the information seen above, we can begin examining the new Lagrangian terms. Starting by the scalar potential, which now depends on two fields as seen in,

$$V(H,\chi) = \mu_1^2 H^\dagger H + \mu_2^2 \chi^*\chi + \lambda_1 (H^\dagger H)^2 + \lambda_2 \left(\chi^*\chi\right)^2 + \lambda_3 \chi^*\chi H^\dagger H \tag{3.1}$$

Being, λ_i, the scalar couplings. This potential must lead to stable vacuum state, for this the scalar potential must be bounded from below (BFB), as to ensure a global minima. Studying the potential on eq. 3.1 we deduce the conditions,

$$4\lambda_1\lambda_2 - \lambda_3^2 > 0 \quad , \quad \lambda_1, \lambda_2 > 0 \tag{3.2}$$

Where the full components of the scalar fields H and χ are given by,

$$H = \frac{1}{\sqrt{2}} \begin{pmatrix} -i\left(\omega_1 - i\omega_2\right) \\ v + (h + iz) \end{pmatrix} \qquad \chi = \frac{1}{\sqrt{2}} \left(x + (h' + iz')\right) \tag{3.3}$$

In these equations we can see h and h' representing the radial quantum fluctuations around the minimum of the potential. These will constitute the physical degrees of freedom associated to the H and H'. There are also four Goldstone directions denoted as ω_1, ω_2, z and z' which are absorbed into longitudinal modes of the $W^\pm$, Z and Z' gauge bosons once spontaneous symmetry breaking (SSB) takes place. After SSB the associated VEVs take the form,

$$\langle H \rangle = \frac{1}{\sqrt{2}} \begin{pmatrix} 0 \\ v \end{pmatrix} \qquad \langle \chi \rangle = \frac{x}{\sqrt{2}} \tag{3.4}$$

From here we can solve the tadpole equations in relation to each of the VEVs as to ensure non-zero VEV, we arrive at,

$$v^2 = \frac{-\lambda_2\mu_1^2 + \frac{\lambda_3}{2}\mu_2^2}{\lambda_1\lambda_2 - \frac{1}{4}\lambda_3^2} > 0 \qquad \text{and} \qquad x^2 = \frac{-\lambda_1\mu_2^2 + \frac{\lambda_3}{2}\mu_1^2}{\lambda_1\lambda_2 - \frac{1}{4}\lambda_3^2} > 0 \tag{3.5}$$

which, when simplified with the bound from bellow conditions yield a simpler set of equations,

$$\lambda_2\mu_1^2 < \tfrac{\lambda_3}{2}\mu_2^2 \qquad \text{and} \qquad \lambda_1\mu_2^2 < \tfrac{\lambda_3}{2}\mu_1^2 \tag{3.6}$$

Note that although λ_1 and λ_2 must be positive to ensure the correct conical shape to the potential, no such conditions exist for the sign of λ_3 , μ_1, and μ_2. However observing equation 3.6 we can infer that only some combinations of signs are impossible,

	$\mu_2^2 > 0$ $\mu_1^2 > 0$	$\mu_2^2 > 0$ $\mu_1^2 < 0$	$\mu_2^2 < 0$ $\mu_1^2 > 0$	$\mu_2^2 < 0$ $\mu_1^2 < 0$
$\lambda_3 < 0$	✗	✓	✓	✓
$\lambda_3 > 0$	✗	✗	✗	✓

Table 3.2: Possible Signs of the potential parameters in (3.1). While the ✓ symbol indicates the existence of solutions for tadpole conditions (3.6), the ✗ indicates unstable configurations.

For our numerical analysis we decided to leave the sign of λ_3 positive, choosing a configuration where both μ parameters are negative. This doesn't directly translate to any real physical consequence. These conditions now established we proceed to investigate the physical states of B-L-SM scalar sector. By first, taking the Hessian matrix evaluated at the vacuum value,

$$\mathbf{M}^2 = \begin{pmatrix} 4\lambda_2 x^2 & \lambda_3 v x \\ \lambda_3 v x & 4\lambda_1 v^2 \end{pmatrix} , \tag{3.7}$$

Moving this matrix to it's physical mass eigen-base, we obtain the following eigenvalues,

$$m^2_{h_{1,2}} = \lambda_1 v^2 + \lambda_2 x^2 \mp \sqrt{(\lambda_1 v^2 - \lambda_2 x^2)^2 + (\lambda_3 x v)^2} , \tag{3.8}$$

The physical basis vectors h_1 and h_2 can then be related to the original fields of gauge eigen-basis h and h' trough a simple rotation matrix:

$$\begin{pmatrix} h_1 \\ h_2 \end{pmatrix} = \mathbf{O} \begin{pmatrix} h \\ h' \end{pmatrix} . \tag{3.9}$$

Being that, the rotation matrix is written as,

$$\mathbf{O} = \begin{pmatrix} \cos\alpha_h & -\sin\alpha_h \\ \sin\alpha_h & \cos\alpha_h \end{pmatrix} . \tag{3.10}$$

The precise mixing angle is represented simply by,

$$\tan 2\alpha_h = \frac{|\lambda_3|\, v v'}{\lambda_1 v^2 - \lambda_2 {v'}^2} \tag{3.11}$$

Although consider it is worth presenting the case of approximate decoupling where, $v/x \ll 1$. In this case scalar masses and mixing angle become particularly simple,

$$\sin\alpha_h \approx \frac{1}{2}\frac{\lambda_3}{\lambda_2}\frac{v}{x} \qquad m^2_{h_1} \approx 2\lambda_1 v^2 \qquad m^2_{h_2} \approx 2\lambda_2 x^2 \tag{3.12}$$

We will see in the context of our numerical results that for our phenomenologically consistent mass scale these equations serve a valid approximation for most of the points.

Gauge Sector

Moving onto the gauge boson and Higgs kinetic terms in the B-L-SM, consider the following portion of the Lagrangian,

$$\mathcal{L}_{U(1)'s} = |D_\mu H|^2 + |D_\mu \chi|^2 - \frac{1}{4}F_{\mu\nu}F^{\mu\nu} - \frac{1}{4}F'_{\mu\nu}F'^{\mu\nu} - \frac{1}{2}\kappa F_{\mu\nu}F'^{\mu\nu} \tag{3.13}$$

where $F^{\mu\nu}$ and $F'^{\mu\nu}$ are the standard field strength tensors, respectively for the hypercharge $\mathrm{U(1)_Y}$ and B minus L $\mathrm{U(1)_{B-L}}$,

$$F_{\mu\nu} = \partial_\mu A_\nu - \partial_\nu A_\mu \qquad \text{and} \qquad F'_{\mu\nu} = \partial_\mu A'_\nu - \partial_\nu A'_\mu\,. \tag{3.14}$$

written in terms of the gauge fields A_μ and A'_μ, respectively. Given that this is a model with two Unitary groups, without a parity symmetry ($\mathbb{Z}_2$) to prevent it, we must consider the possible mixing in between them. In this work we parametrized this mixing trough a parameter κ.

The Abelian part of the covariant derivative in equation 3.13 is given by,

$$D_\mu \supset i g_1 Y A_\mu + i g'_1 Y_{\mathrm{B-L}} A'_\mu\,, \tag{3.15}$$

with g_1 and g'_1 being the $\mathrm{U(1)_Y}$ and $\mathrm{U(1)_{B-L}}$ the gauge couplings with the Y and $B-L$ charges are specified in Tab. 3.1. However it is convenient to rewrite the gauge kinetic terms in the canonical form, i.e.

$$F_{\mu\nu}F^{\mu\nu} + F'_{\mu\nu}F'^{\mu\nu} + 2\kappa F_{\mu\nu}F'^{\mu\nu} \to B_{\mu\nu}B^{\mu\nu} + B'_{\mu\nu}B'^{\mu\nu}\,. \tag{3.16}$$

A generic orthogonal transformation in the field space does not eliminate the kinetic mixing term. So, in order to satisfy Eq. (3.16) an extra non-orthogonal transformation should be imposed such that Eq. (3.16) is realized. Taking $\kappa = \sin\alpha$, a suitable redefinition of fields $\{A_\mu, A'_\mu\}$ into $\{B_\mu, B'_\mu\}$ that eliminates κ-term according to Eq. (3.13) can be cast as

$$\begin{pmatrix} A_\mu \\ A'_\mu \end{pmatrix} = \begin{pmatrix} 1 & -\tan\alpha \\ 0 & \sec\alpha \end{pmatrix} \begin{pmatrix} B_\mu \\ B'_\mu \end{pmatrix}, \tag{3.17}$$

Note there is a limit without kinetic mixing where $\alpha = 0$. Note that this transformation is generic and valid for any basis in the field space. The transformation (3.17) results in a modification of the covariant derivative that acquires two additional terms encoding the details of the kinetic mixing, i.e.

$$D_\mu \supset \partial_\mu + i\left(g_Y\, Y + g_B Y\, Y_{B-L}\right) B_\mu + i\left(g_{B-L}\, Y_{B-L} + g_{YB}\, Y\right) B'_\mu\,, \tag{3.18}$$

where the gauge couplings take the form

$$\begin{cases} g_Y = g_1 \\ g_{B-L} = g'_1 \sec\alpha \\ g_{YB} = -g_1 \tan\alpha \\ g_{BY} = 0 \end{cases}, \tag{3.19}$$

which is the standard convention in the literature. Note this definition is merely to simply the equations and has no physical impact. We will later see that this kinetic mixing is a desired feature and why stabilizing it with a $\mathbb{Z}_{\not E}$ symmetry would be detrimental in terms of depth. The resulting mixing between the neutral gauge fields including Z' can be represented as follows

$$\begin{pmatrix} \gamma_\mu \\ Z_\mu \\ Z'_\mu \end{pmatrix} = \begin{pmatrix} \cos\theta_W & \sin\theta_W & 0 \\ -\sin\theta_W\cos\theta'_W & \cos\theta_W\cos\theta'_W & \sin\theta'_W \\ \sin\theta_W\sin\theta'_W & -\cos\theta'_W\sin\theta'_W & \cos\theta'_W \end{pmatrix} \begin{pmatrix} B_\mu \\ A^3_\mu \\ B'_\mu \end{pmatrix} \tag{3.20}$$

where θ_W is the weak mixing angle and θ'_W is defined as

$$\sin(2\theta'_W) = \frac{2g_{YB}\sqrt{g^2+g_Y^2}}{\sqrt{(g_{YB}^2+16(\frac{x}{v})^2 g_{B-L}^2 - g^2 - g_Y^2)^2 + 4g_{YB}^2(g^2+g_Y^2)}}\,, \tag{3.21}$$

in terms of g and g_Y being the $SU(2)_L$ and U_Y gauge couplings, respectively. In the physically relevant limit, $v/x \ll 1$, the above expression greatly simplifies leading to

$$\sin\theta'_W \approx \frac{1}{16}\frac{g_{YB}}{g_{B-L}}\left(\frac{v}{x}\right)^2\sqrt{g^2+g_Y^2}\,, \tag{3.22}$$

up to $(v/x)^3$ corrections. In the limit of no kinetic mixing, i.e. $g_{YB} \to 0$, there is no mixture of Z' and SM gauge bosons.

Note, the kinetic mixing parameter θ'_W has rather stringent constraints from Z pole experiments both at the Large Electron-Positron Collider (LEP) and the Stanford Linear Collider (SLC), restricting its value to be smaller than 10^{-3} approximately, which we set as an upper bound in our numerical analysis. Expanding the kinetic terms $|D_\mu H|^2 + |D_\mu \chi|^2$ around the vacuum one can extract the following mass matrix for vector bosons

$$m_V^2 = \frac{v^2}{4}\begin{pmatrix} g^2 & 0 & 0 & 0 & 0 \\ 0 & g^2 & 0 & 0 & 0 \\ 0 & 0 & g^2 & -gg_Y & -gg_{YB} \\ 0 & 0 & -gg_Y & g_Y^2 & g_Y g_{YB} \\ 0 & 0 & -gg_{YB} & g_Y g_{YB} & g_{YB}^2 + 16\left(\frac{x}{v}\right)^2 g_{B-L}^2 \end{pmatrix} \tag{3.23}$$

whose, first set eigenvalues read,

$$m_A = 0\,, \qquad m_W = \tfrac{1}{2}vg \tag{3.24}$$

corresponding to the expected physical photon and $W^\pm$ bosons. While the following set,

$$m_{Z,Z'} = \sqrt{g^2+g_Y^2}\cdot\frac{v}{2}\sqrt{\frac{1}{2}\left(\frac{g_{YB}^2+16(\frac{x}{v})^2 g_{\rm BL}^2}{g^2+g_Y^2}+1\right) \mp \frac{g_{YB}}{\sin(2\theta'_W)\sqrt{g^2+g_Y^2}}}\,. \tag{3.25}$$

correspond to two neutral massive vector bosons, with one of them, not necessarily the lightest, representing the SM-like Z boson. It follows from LEP and SLC constraints on θ'_W, that Eq. (3.22) also implies that either g_{YB} or the ratio $\frac{v}{x}$ are small. In this limit, Eq. (3.25) simplifies to

$$m_Z \approx \tfrac{1}{2} v \sqrt{g^2 + g_Y^2} \qquad \text{and} \qquad m_{Z'} \approx 2 g_{B-L} x \,, \tag{3.26}$$

where the $m_{Z'}$ depends only on the SM-singlet VEV ,x and on the $\mathrm{U(1)_{B-L}}$ gauge coupling and will be attributed to a heavy Z' state, while the light Z-boson mass corresponds to its SM value.

The Yukawa sector

One of the key features of the B-L-SM is the presence of non-zero neutrino masses. In its minimal version, such masses are generated via a type-I seesaw mechanism, thus producing a very light neutrino for each of the three known neutrino flavours, and a corresponding very heavy neutrino for each, which has yet to be observed. In the type-I seesaw mechanism the mixing of neutrinos fields is written with similar shape to,

$$\left(\begin{array}{c|c} 0 & A \\ \hline A & B \end{array}\right) \tag{3.27}$$

This system would have a set eigenvalues written as,

$$\lambda_{\pm} = \frac{B \pm \sqrt{B^2 + 4A}}{2} \tag{3.28}$$

Investigating the nature of this set of eigenvalues allows us to understand the see-saw. The mean of these values being always equal to $|B|$, if one value goes up, another goes down, like a see-saw. Note B, generally is the Majorana mass terms, and is generally very large in comparison to the cross interaction terms. Given this the smaller eigenstate to be approximate,

$$\lambda_{-} \approx \frac{A^2}{B} \tag{3.29}$$

This mechanism serves to explain why the neutrino masses are so small.

The total Yukawa Lagrangian of the model reads,

$$\mathcal{L}_f = -Y_u^{ij} \overline{q_{\mathrm{Li}}} u_{\mathrm{Rj}} \widetilde{H} - Y_d^{ij} \overline{q_{\mathrm{Li}}} d_{\mathrm{Rj}} H - Y_e^{ij} \overline{\ell_{\mathrm{Li}}} e_{\mathrm{Rj}} H - Y_\nu^{ij} \overline{\ell_{\mathrm{Li}}} \nu_{\mathrm{Rj}} \widetilde{H} - \frac{1}{2} Y_\chi^{ij} \overline{\nu_{\mathrm{Ri}}^c} \nu_{\mathrm{Rj}} \chi + \mathrm{c.c.} \tag{3.30}$$

Notice the explicit lack of Majorana neutrino mass terms of the form $M \overline{\nu_R^c} \nu_R$. These explicitly violate the $\mathrm{U(1)_{B-L}}$ symmetry and are therefore not present. In Eq. (3.30), Y_u, Y_d and Y_e are the 3×3 Yukawa matrices that reproduce the quark and charged lepton sector exactly the same way as in the SM, while Y_ν and Y_χ are the new Yukawa matrices responsible for the generation of right handed neutrino masses and mixing with left handed fields. In particular, one can write,

$$\mathbf{m}_{\nu_l}^{Type-I} = \frac{1}{\sqrt{2}}\frac{v^2}{x}\mathbf{Y}_\nu^t\mathbf{Y}_\chi^{-1}\mathbf{Y}_\nu\,, \tag{3.31}$$

for light ν_l neutrino masses, whereas the heavy ν_h ones are given by

$$\mathbf{m}_{\nu_h}^{Type-I} \approx \frac{1}{\sqrt{2}}\mathbf{Y}_\chi x\,, \tag{3.32}$$

where we have assumed a flavour diagonal basis.

Note that the smallness of light neutrino masses imply that either the x VEV is very large or (if we fix it to be at the $\mathcal{O}\,(TeV)$ scale and $\mathbf{Y}_\chi \sim \mathcal{O}\,(1)$) the corresponding Yukawa coupling should be tiny, $\mathbf{Y}_\nu < 10^{-6}$. It is clear that the low scale character of the type-I seesaw mechanism in the minimal B-L-SM is *faked* by small Yukawa couplings to the Higgs boson. A more elegant description was proposed in Ref. [39] where small SM neutrino masses naturally result from an inverse seesaw mechanism. In this work, however, we will not study the neutrino sector and thus, for an improved efficiency of our numerical analysis of Z' observables, it will be sufficient to fix the Yukawa couplings to $\mathbf{Y}_\chi = 10^{-1}$ and $\mathbf{Y}_\nu = 10^{-7}$ values such that the three lightest neutrinos lie in the sub-eV domain.

I think I should show more of the diagonalization process? This last part seems barren

3.2 Numerical Results

Before we begin this section consider that our colleges in a recent work tested the state of the art at the LHC for low mass Z' boson [40]. In particular from 0.2GeV to 200GeV. As for slightly heavier Z' masses beyond $m_{Z'} \gtrsim 100$ GeV, the combined effect of the electroweak precision observables and the ATLAS searches for Drell-Yan Z' production decaying into di-leptons, i.e. $pp \to Z' \to ee, \mu\mu$ [1], is also finely investigated. We then endeavoured to achieve a complementary study where we investigated the case of very heavy Z' bosons.

Our goal was to discover if it was still possible to, with such a heavy Z' boson, limited by LHC, with such a heavily constrained kinetic mixing, to have any significant phenomenological impact asides from simply a yet to be observed boson. This was chiefly done by the investigation of the $(g-2)_\mu$ anomaly. We examine the relations that this anomaly has with the parameter space, such as gauge couplings, as well as the extra scalar mass. The $(g-2)_\mu$ anomaly refers to the discrepancy between the measured anomalous magnetic moment of the muon, $a_\mu^{\text{exp}} \equiv \frac{1}{2}\,(g-2)_\mu^{\text{exp}}$, and its theoretical prediction, $a_\mu^{\text{SM}} \equiv \frac{1}{2}\,(g-2)_\mu^{\text{SM}}$, which reads [17]

$$\Delta a_\mu = a_\mu^{\text{exp}} - a_\mu^{\text{SM}} = 268(63)(43) \times 10^{-11} \tag{3.33}$$

with numbers in brackets denoting experimental and theoretical errors, respectively. This represents a tension of 3.5 standard deviations from the combined 1σ error and is calling for new physics effects beyond the SM theory.

There is a strong possibility that through radiative corrections a new gauge bosons could explain this deviation [41]. In fact a version of this study has already been performed in the supersymmetrical version of the B-L-SM [42, 43].

3.2.1 The scanning apparatus

The numerical data presented in this section of our work was generated thorough a large chain of nested scripts. These were created as a possible first generation of a scanning framework for generic phenomenological models. This machinery was adapted to the 3HDM numerical scan so this introduction will be glossed over in the 3HDM section, as much remained the same.

The scripts were a mixture of Linux bash and Python 3 scripts, and utilize the `SPheno 4.0.3` [44, 45], `SARAH 4.13.0` [46, 47], `HiggsBounds 4.3.1` [48], `HiggsSignals 1.4.0` [49] and `MadGraph5_aMC@NLO 2.6.2` [50] programs/packages.

These scripts generate a Monte-Carlo type scan through a desired parameter space. Unless introduced, all non-relevant physical constants and parameters are defined in a way as to keep the observed gauge, lepton and quark structure consistent with the SM. Skipping a bit ahead, as a example, for the B-L-SM scan our scanning routine randomly samples parameter space points according to the ranges in Tab. 3.3 while keeping things like Higgs doublet VEV and Weinberg angle to reproduce the correct W and Z structure.

Given the randomness in our scan, we can reach unphysical, or nonsensical regions, that contain objects like tachyonic scalar masses un-renormalizable quantities, divergent radiative corrections etc. These points must be rejected before even considering experimental constraints. This is done by `SPheno`, rejecting any point generated with unphysical parameters.

We could consider this our first layered check. While a second layer of tests include the phenomenological studies we shall perform. This is the region where we confront the surviving scenarios with experimental data. Such as precision measurements from the oblique S, T, U parameters and constraining the Higgs Sector to reproduce the observed signal seen in the LHC in 2012. The latter is made automatically trough the package `HiggsBounds 4.3.1` that shall be used to apply a 95% C.L. exclusion limit cut on a new scalar particle, h_2, while `HiggsSignals 1.4.0` is used to calculate and later check, through a χ^2 distribution, the probability for consistency with the observed Higgs boson signal data. To calculate these variables `HiggsBounds 4.3.1` and `HiggsSignals 1.4.0` are provided all scalar masses, total decay widths, Higgs decay branching ratios as well as the SM-normalized effective Higgs couplings to fermions and bosons squared (that are needed for analysis of the Higgs boson production cross sections). For details about this calculation, see Ref. [48].

All data generated for a point in the parameter space is generated by `SPheno`. `SPheno` is a particle spectrum generator code written in Fortran 90. It's emphasis on easy generalisability and speed made it a natural part of our numerical analysis. It takes information about our models Lagrangian, such as fields, charges and fundamental symmetries, and creates a executable file capable of quickly generating a spectrum file with all details regarding mass, decay and flavour observables information in the standardized SUSY Les-Houches accord format. All generated spectrums are processed and stored. This Lagrangian information is fed to `SPheno` also in standardized format automatically generated by a Mathematica packaged designed for such purposes called `SARAH`.

On a third and final layer of phenomenological tests we have studied the viability of the surviving scenarios from the perspective of direct collider searches for a new Z' gauge boson. We have used, the popular `MadGraph5_aMC@NLO`, to compute the Z' Drell-Yan production cross section and subsequent decay into the first and second-generation leptons, i.e. $\sigma\,(pp \to Z') \times B\,(Z' \to \ell\ell)$ with $\ell = e,\ \mu$, and then compared our results to the most recent ATLAS exclusion bounds from the LHC runs at the center-of-mass energy $\sqrt{s} = 13$ TeV [1]. The `SPheno` SLHA output files were used as parameter cards for `MadGraph5_aMC@NLO`, where the information required to calculate $\sigma\,(pp \to Z') \times B\,(Z' \to \ell\ell)$, such as the Z' boson mass, its total width and decay branching ratios into lepton pairs, is provided. The lepton anomalous magnetic moments $(g-2)_\ell/2 \equiv a_\ell$ are calculated in `SPheno` at one-loop order. In the B-L-SM, new physics (NP) contributions to a_μ, denoted as $\Delta a_\mu^{\mathrm{NP}}$ in what follows, can emerge from the diagrams containing Z' or h_2 propagators, as a example consider Figs. 3.3.

3.2.2 Numerical discussion

For the B-L-SM scan our scanning routine randomly samples parameter space points according to the ranges in Tab. 3.3.

λ_1	$\lambda_{2,3}$	$g_{\mathrm{B-L}}$	g_{YB}	x [TeV]
$[10^{-2},\ 10^{0.5}]$	$[10^{-8},\ 10]$	$[10^{-8},\ 10]$	$[10^{-8},\ 10]$	$[0.5,\ 20.5]$

Table 3.3: Parameter scan ranges used in our analysis. Note that the value of λ_1 is mostly constrained by the tree-level Higgs boson mass given in Eq. (3.12).

Keeping the remaining free parameters of the model to be in agreement with the Standard Model. The presence of new bosons in the theory can lead to large deviations in EW precision observables. Typically, the most stringent constraints of the scalar sector emerge from the oblique S, T, U parameters, which are also calculated by `SPheno`. Current precision measurements provide the allowed regions,

$$S = 0.02 \pm 0.10\,, \qquad T = 0.07 \pm 0.12\,, \qquad U = 0.00 \pm 0.09 \tag{3.34}$$

where S-T are 92% correlated, while S-U and T-U are -66% and -86% anti-correlated, respectively. We compare our results with the EW fit in Eq. (3.34) and require consistency with the best fit point within a 95% C.L. ellipsoid (see Ref. [51] for further details about this method). We show in Fig. 3.1 our results in the ST (left) and TU (right) planes where black points are consistent with EW precision observables at 95% C.L. whereas grey ones lie outside the corresponding ellipsoid of the best fit point and, thus, the first points to be excluded in our analysis.

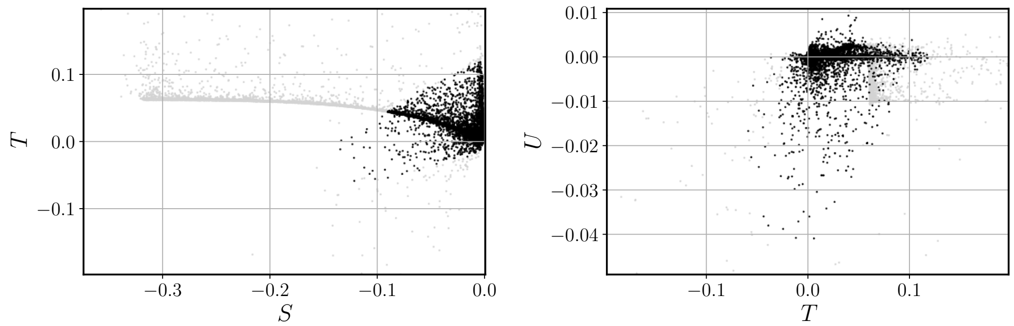

Figure 3.1: Scatter plots for EW precision observables showing the ST (left) and TU (right) planes. Accepted points lying within a 95% C.L. ellipsoid of the best fit point are represented in black whereas grey points are excluded.

As stated we confront the surviving scenarios, black points in Fig. 3.1, with collider bounds. In particular 95% C.L. exclusion limits on a new scalar particle and check for consistency with the observed Higgs boson at 3σ. From here we move onto the third layer of phenomenological tests we have studied the viability of the surviving scenarios from the perspective of direct collider searches for a new Z' gauge boson at the most recent collider experiments. Let us now discuss the phenomenological properties of the B-L-SM model. First, we focus on the current collider constraints and study their impact on both the scalar and gauge sectors.

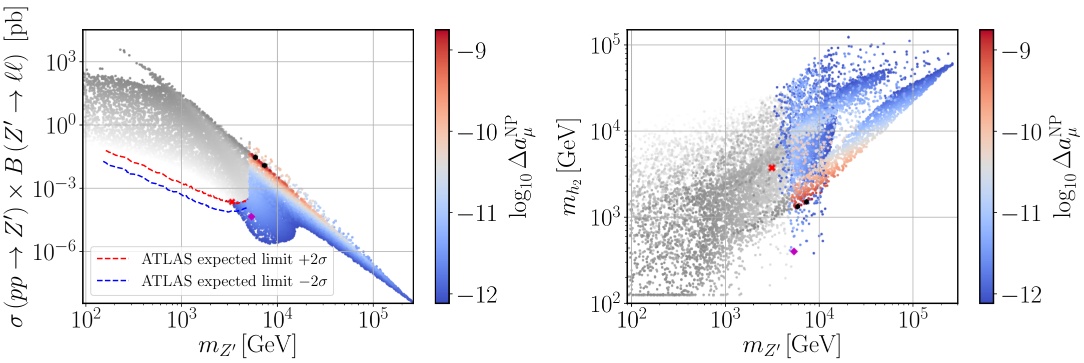

Figure 3.2: Scatter plots showing the Z' Drell-Yan production cross section times the decay branching ratio into a pair of electrons and muons (left panel) and the new scalar mass m_{h_2} (right panel) as functions of $m_{Z'}$ and the new physics (NP) contributions to the muon Δa_μ anomaly. Coloured points have survived all theoretical and experimental constraints while grey points are excluded by direct Z' searches at the LHC. The region between the two dashed lines represents the current ATLAS expected limit on the production cross section times branching ratio into a pair of leptons at 95% C.L. and is taken from the *Brazilian* plot in Fig. 4 of Ref. [1]. The four highlighted points in both panels denote the benchmark scenarios described in detail in Tab. 3.4.

We show in Fig. 3.2 the scenarios generated in our parameter space scan (see Tab. 3.3) that have passed all theoretical constraints such as boundedness from below, unitarity and EW precision tests, are compatible with the SM Higgs data and where a new visible scalar h_2 is unconstrained by the direct collider searches. On the left panel, we show the Z' production cross section times its branching ratio to the first- and second-generation leptons, $\sigma B \equiv \sigma\,(pp \to Z') \times B\,(Z' \to \ell\ell)$ with $\ell = e, \mu$, as a function of the new vector boson mass and the new physics contribution to the muon anomalous magnetic moment $\Delta a_\mu^{\mathrm{NP}}$ (colour scale). On the right panel, we show the new scalar mass as a function of the same observables. All points above the red dashed line are excluded at 95% C.L. by the upper expected limit on Z' direct searches at the LHC by the ATLAS experiment and are represented in grey shades. Darker shades denote *would-be-scenarios* with larger values of $\Delta a_\mu^{\mathrm{NP}}$ while the smaller contributions to the muon $(g-2)_\mu/2$ anomaly are represented with the lighter shades. The region between the two dashed lines corresponds to the Z' ATLAS limit with a 2σ uncertainty represented by the yellow band in Fig. 4 of [1]. Provided that the observed limit by the ATLAS detector lies within this region we have taken a conservative approach and accepted all points whose σB value lies below the red dashed line (upper limit) in Fig. 3.2. The blue dashed line, which corresponds to the stricter 2σ lower bound, is only shown for completeness of information. The red cross in our figures signals the lightest Z' found in our scan which we regard as a possible early-discovery (or early-exclusion) benchmark point in the forthcoming LHC runs. Such a benchmark point is shown in the first line of Tab. 3.4. On the right panel, we notice that the new scalar bosons can become as light as $380 - 400$ GeV, but with Z' masses in the range of $5 - 9$ TeV. We highlight with a magenta diamond the benchmark point with the lightest Z' boson within this range. This point is shown in the second line of Tab. 3.4.

$m_{Z'}$	m_{h_2}	x	$\log_{10}\Delta a_\mu^{\rm NP}$	σB	θ'_W	α_h	$g_{\text{B-L}} \simeq g^{\ell\ell Z'}$
3.13	3.72	15.7	-12.1	2.22×10^{-4}	≈ 0	5.67×10^{-5}	0.0976
5.37	0.396	9.10	-11.7	4.23×10^{-5}	2.55×10^{-7}	9.44×10^{-7}	0.302
7.35	1.49	0.321	-8.75	0.0115	1.83×10^{-7}	1.20×10^{-6}	3.15
5.91	1.32	0.335	-8.78	0.0285	1.30×10^{-4}	1.04×10^{-5}	2.94

Table 3.4: A selection of four benchmark points represented in Figs. 3.2, 3.4 to 3.6. The $m_{Z'}$, m_{h_2} and x parameters are given in TeV. The first line represents a point with light h_2 while the second line shows the lightest allowed Z' boson found in our scan. The last two lines show two points that reproduce the observed value of the muon $(g-2)$ within 1σ uncertainty.

Implications of direct Z' searches at the LHC for the $(g-2)_\mu$ anomaly

Looking again to Fig. 3.2 (left panel), we see that there is a thin dark-red stripe where $\Delta a_\mu^{\rm NP}$ explains the observed anomaly shown in Eq. (3.33) for a range of $m_{Z'}$ boson masses approximately between 5 TeV and 20 TeV. This region is particularly interesting as it can be partially probed by the forthcoming LHC runs or at future colliders. If a Z' boson discovery remains elusive for such a mass range, it can exclude a possibility of explaining the muon $(g-2)_\mu$ anomaly in the context of the B-L-SM. It is also worth noticing that such preferred $\Delta a_\mu^{\rm NP}$ values represent a small island in the right plot of Fig. 3.2 where the new scalar boson mass is restricted to the range of 1 TeV $< m_{h_2} <$ 4 TeV.

New physics contributions $\Delta a_\mu^{\rm NP}$ to the muon anomalous magnetic moment are given at one-loop order by the Feynman diagrams depicted in Fig. 3.3. Since the couplings of a

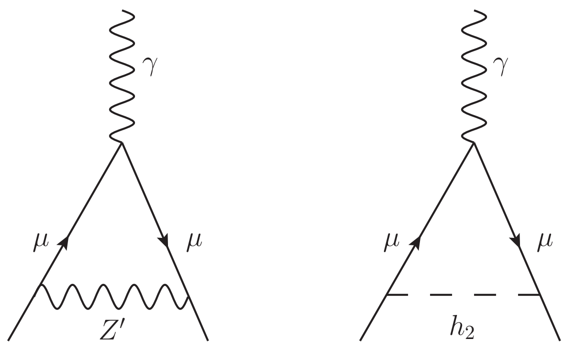

Figure 3.3: One-loop diagrams contributing to $\Delta a_\mu^{\rm NP}$ in the B-L-SM.

new scalar h_2 to the SM fermions are suppressed by a factor of $\sin\alpha_h$, which we find to be always smaller than 0.08 as can be seen in the bottom panel of Fig. 3.4, the right diagram in Fig. 3.3, which scales as $\Delta a_\mu^{h_2} \propto \frac{m_\mu^2}{m_{h_2}^2}\left(y_\mu \sin\alpha_h\right)^2$ with $\sin^2\alpha_h < 0.0064$ and $y_\mu = Y_e^{22}$, provides sub-leading contributions to Δa_μ. Furthermore, as we show in the top-left panel of Fig. 3.4 the new scalar boson mass, which we have found to satisfy $m_{h_2} \gtrsim 380$ GeV, is not light enough to compensate the smallness of the scalar mixing angle. Conversely, and recalling that all fermions in the B-L-SM transform non-trivially under $\mathrm{U}(1)_{\mathrm{B-L}}$, the new Z' boson can have sizeable couplings to fermions via gauge interactions proportional to $g_{\mathrm{B-L}}$. Therefore, the left diagram in Fig. 3.3 provides the leading contribution to the $(g-2)_\mu$ in the model under consideration. In particular, $\Delta a_\mu^{Z'}$ is given by [52]

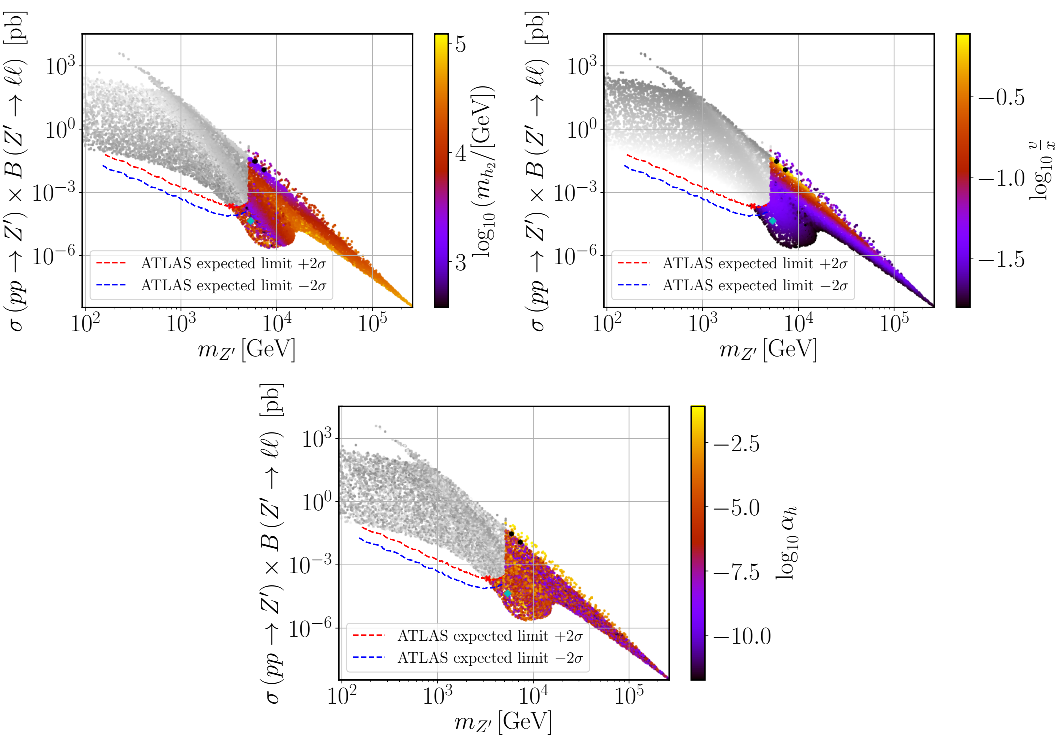

Figure 3.4: Scatter plots showing the Z' Drell-Yan production cross section times the decay branching ratio into a pair of electrons and muons in terms of the $m_{Z'}$ boson mass. The colour gradation represents the new scalar mass (top-left), the ratio between the EW- and $\mathrm{U}(1)_{\mathrm{B-L}}$-breaking VEVs (top-right) and the scalar mixing angle (bottom). The grey points are excluded by direct Z' searches at the LHC. The four benchmark points in Tab. 3.4 are represented by the black dots (last two rows), cyan diamond (first row) and red cross (second row).

$$\Delta a_\mu^{Z'} = \frac{1}{12\pi^2}\frac{m_\mu^2}{m_{Z'}^2}\left(3 g_{\mathrm{L}}^{\mu\mu Z'} g_{\mathrm{R}}^{\mu\mu Z'} - {g_{\mathrm{L}}^{\mu\mu Z'}}^2 - {g_{\mathrm{R}}^{\mu\mu Z'}}^2\right) \tag{3.35}$$

where the left- and right-chiral projections of the charged lepton couplings to the Z' boson,

$g_{\mathrm{L}}^{\ell\ell Z'}$ and $g_{\mathrm{R}}^{\ell\ell Z'}$, respectively, can be approximated as follows

$$\begin{aligned} g_{\mathrm{L}}^{\ell\ell Z'} &\simeq g_{\mathrm{B-L}} + \tfrac{1}{32}\left(\tfrac{v}{x}\right)^2 \tfrac{g_{\mathrm{YB}}}{g_{\mathrm{B-L}}}\left[g_{\mathrm{Y}}^2 - g^2 + 2g_{\mathrm{Y}}g_{\mathrm{YB}}\right] , \\ g_{\mathrm{R}}^{\ell\ell Z'} &\simeq g_{\mathrm{B-L}} + \tfrac{1}{16}\left(\tfrac{v}{x}\right)^2 \tfrac{g_{\mathrm{YB}}}{g_{\mathrm{B-L}}}\left[g_{\mathrm{Y}}^2 + g_{\mathrm{Y}}g_{\mathrm{YB}}\right] , \end{aligned} \tag{3.36}$$

to the second order in v/x-expansion. If $v/x \ll 1$, corresponding to the darker shades of the color scale in the top-right panel of Fig. 3.4, we can further approximate

$$g_{\mathrm{L}}^{\ell\ell Z'} \simeq g_{\mathrm{R}}^{\ell\ell Z'} \simeq g_{\text{B-L}} , \tag{3.37}$$

such that the muon anomalous magnetic moment gets significantly simplified to

$$\Delta a_\mu^{Z'} \simeq \frac{g_{\text{B-L}}^2}{12\pi^2}\frac{m_\mu^2}{m_{Z'}^2} . \tag{3.38}$$

Similarly, for the yellow band, which corresponds to the region where $\Delta a_\mu^{\mathrm{NP}}$ is maximized (see top-left panel of Fig. 3.2), a large value of the $\mathrm{U}(1)_{\mathrm{B-L}}$ gauge coupling also allows one to simplify Eq. (3.35) reducing it to the form of Eq. (3.38). This is in fact what we have observed and, for the yellow band region, we see in the bottom panel of Fig. 3.5 that $g_{\text{B-L}} \simeq 3$. A sizeable value of $g_{\text{B-L}}$ is indeed what is contributing to the enhancement of $\Delta a_\mu^{\mathrm{NP}}$, in particular, for the red region in both panels of Fig. 3.2. We show in the third and fourth lines of Tab. 3.4 the two benchmark points that better reproduce the muon anomalous magnetic moment represented by two black dots in Figs. 3.2, 3.4 to 3.6.

In fact, a close inspection of Fig. 3.2 (left panel) and Fig. 3.4 (top-right panel) reveals an almost one-to-one correspondence between the colour shades. This suggests that $\Delta a_\mu^{Z'}$ must somehow be related to the VEV ratio v/x. To understand this behaviour, let us also look to Fig. 3.5 (top-right panel) where we see that the kinetic-mixing gauge coupling g_{YB} is typically very small apart from two green bands where it can become of order $\mathcal{O}(1)$. Interestingly, whenever g_{YB} becomes sizeable, $v/x \ll 1$ is realised, which means that Eq. (3.26) is indeed a good approximation as was argued above. It is then possible to eliminate $g_{\text{B-L}}$ from Eq. (3.38) and rewrite it as

$$\Delta a_\mu^{Z'} \simeq \frac{y_\mu^2}{96\pi^2}\left(\frac{v}{x}\right)^2 , \tag{3.39}$$

which explains the observed correlation between both Fig. 3.2 (left panel) and Fig. 3.4 (top-right panel) and, for instance, the thin red stripe of points compatible with a full description of the muon $(g-2)_\mu/2$ anomaly. Note that this simple and illuminating relation becomes valid as a consequence of the heavy Z' mass regime, in combination with the smallness of the θ_W' mixing angle required by LEP constraints. Indeed, while we have not imposed any strong restriction on the input parameters of our scan (see Tab. 3.3), Eq. (3.22) necessarily implies that both g_{YB} and v/x cannot be simultaneously sizeable in agreement with what is seen in Fig. 3.5 (top-left panel) and Fig. 3.4 (top-right panel). The values of θ_W' obtained in our scan are shown in the top-right panel of Fig. 3.5.

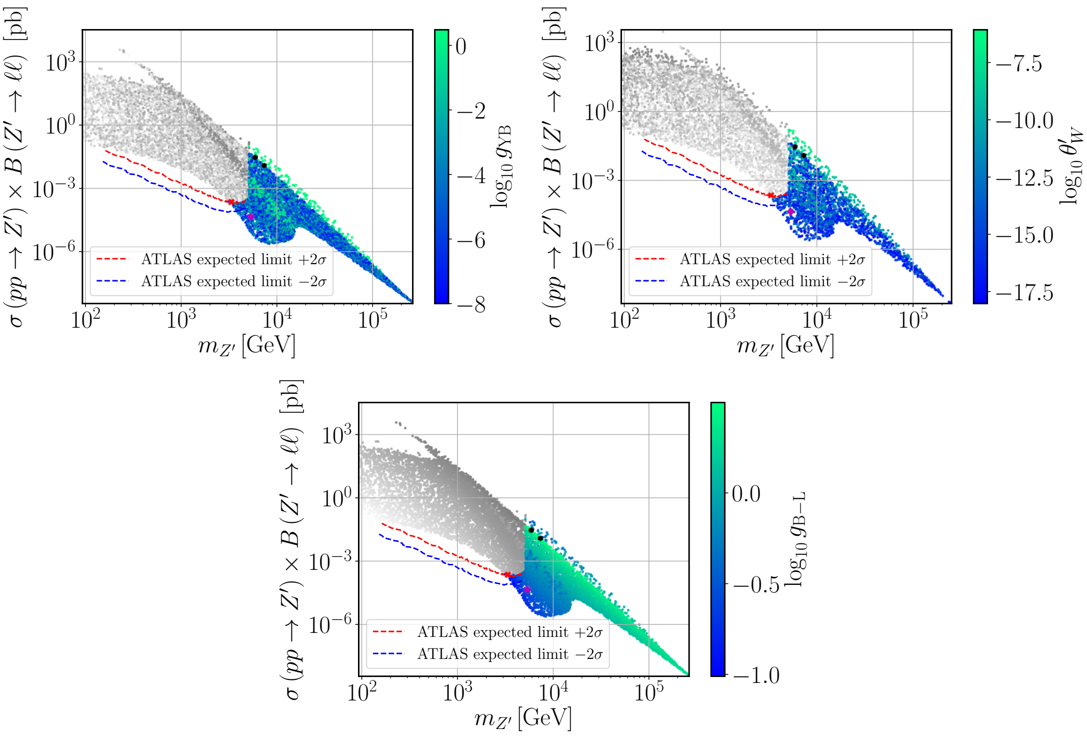

Figure 3.5: The same as in Fig. 3.4 but with the colour scale representing the gauge-mixing parameters $g_{\rm YB}$ (top-left) and θ'_W (top-right), and the $\mathrm{U(1)_{B-L}}$ gauge coupling (bottom).

For completeness, we show in Fig. 3.6 the physical couplings of Z' to muons (top panels) and to $W^\pm$ bosons (bottom panel). Note that, for the considered scenarios, the latter can be written as

$$g^{WWZ'} \simeq \frac{1}{16}\frac{g_{\text{YB}}}{g_{\text{B-L}}}\left(\frac{v}{x}\right)^2 . \tag{3.40}$$

While both $g_{\text{B-L}}$ and the ratio v/x provide a smooth continuous contribution in the $\sigma B - m_{Z'}$ projection of the parameter space, the observed blurry region in $g^{WWZ'}$ is correlated with the one in the top-left panel of Fig. 3.5 as expected from Eq. (3.40). On the other hand, the couplings to leptons $g_{\rm L,R}^{\ell\ell Z'}$ exhibit a strong correlation with $g_{\text{B-L}}$ in Fig. 3.5, in agreement with our discussion above and with Eq. (3.37).

Barr-Zee type contributions

To conclude our analysis, one should note that the two-loop Barr-Zee type diagrams [53] are always sub-dominant in our case. To see this, let us consider the four diagrams shown in Fig. 3.7. The same reason that suppresses the one-loop h_2 contribution in Fig. 3.3 is also responsible for the suppression of both the top-right and bottom-right diagrams in Fig. 3.7 (for details see e.g. Ref. [54]). Recall that the coupling of h_2 to the SM particles is proportional to the scalar mixing angle α_h, which is always small (or very small) as we can

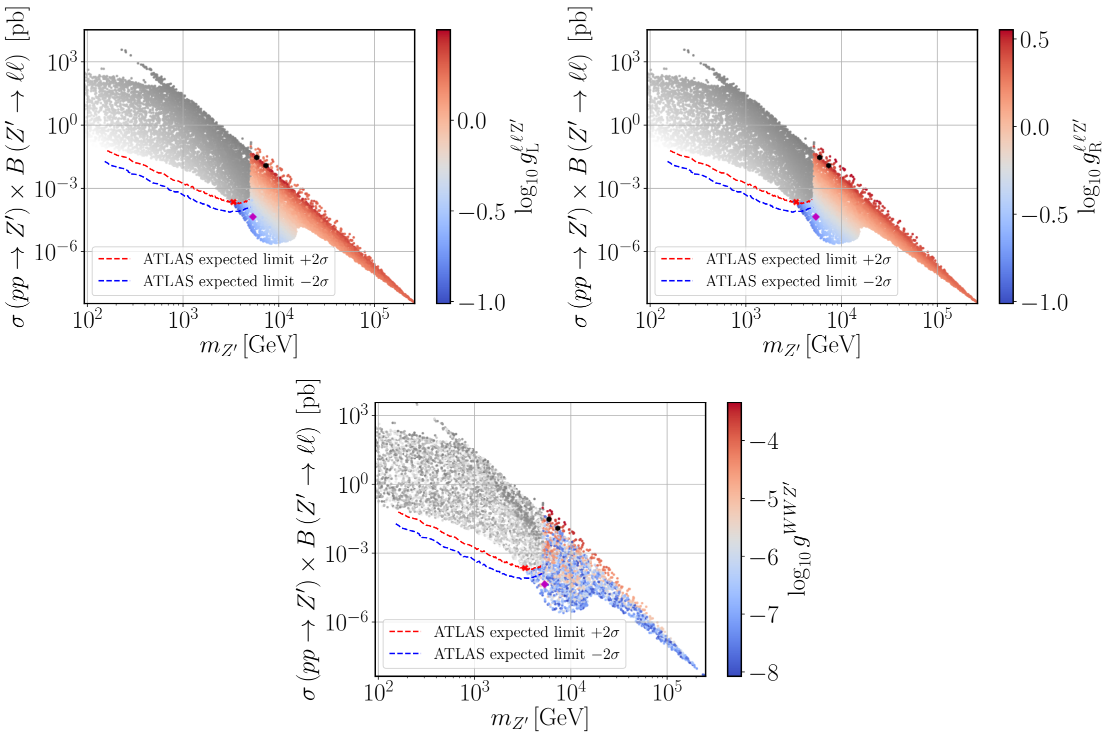

Figure 3.6: The same as in Fig. 3.4 but with the colour scale representing the coupling of leptons to the Z' (top panels) and the coupling of W bosons to Z'.

---

see in Fig. 3.4. An analogous effect is present in the diagram involving a W-loop, where a vertex proportional to $g^{WWZ'}$ suppresses such a contribution. The only diagram that might play a sizeable role is the top-left one where the couplings of Z' to both muons and top quarks are not negligible.

Let us then estimate the size of the first diagram in Fig. 3.7. This type of diagrams were already calculated in Ref. [55] but for the case of a SM Z-boson. Since the same topology holds for the considered case of B-L-SM too, if we trade Z by the new Z' boson, the contribution to the muon $(g-2)_\mu$ anomaly can be rewritten as

$$\Delta a_\mu^{\gamma Z'} = -\frac{g^2 g_{\text{B-L}}^2 m_\mu^2 \tan^2\theta_W}{1536\pi^4}\left(g_{\rm L}^{ttZ'} - g_{\rm R}^{ttZ'}\right) \mathrm{T}_7\left(m_{Z'}^2, m_t^2, m_t^2\right) , \tag{3.41}$$

where $g_{\rm L,R}^{ttZ'}$, calculated in `SARAH`, are the left- and right-chirality projections of the Z' coupling to top-quarks, given by

$$\begin{aligned} g_{\rm L}^{ttZ'} &= -\frac{g_{\text{B-L}}}{3}\cos\theta'_W + \frac{g}{2}\cos\theta_W\sin\theta'_W - \frac{g_{\rm Y}}{6}\sin\theta_W\sin\theta'_W - \frac{g_{\rm YB}}{3}\sin\theta_W\sin\theta'_W\,, \\ g_{\rm R}^{ttZ'} &= -\frac{g_{\text{B-L}}}{3}\cos\theta'_W - \frac{2g_{\rm Y}}{3}\sin\theta_W\sin\theta'_W - \frac{g_{\rm YB}}{3}\sin\theta_W\sin\theta'_W\,. \end{aligned} \tag{3.42}$$

The loop integral $\mathrm{T}_7\left(m_{Z'}^2, m_t^2, m_t^2\right)$ was determined in Ref. [55] and, in the limit $m_{Z'} \gg m_t$,

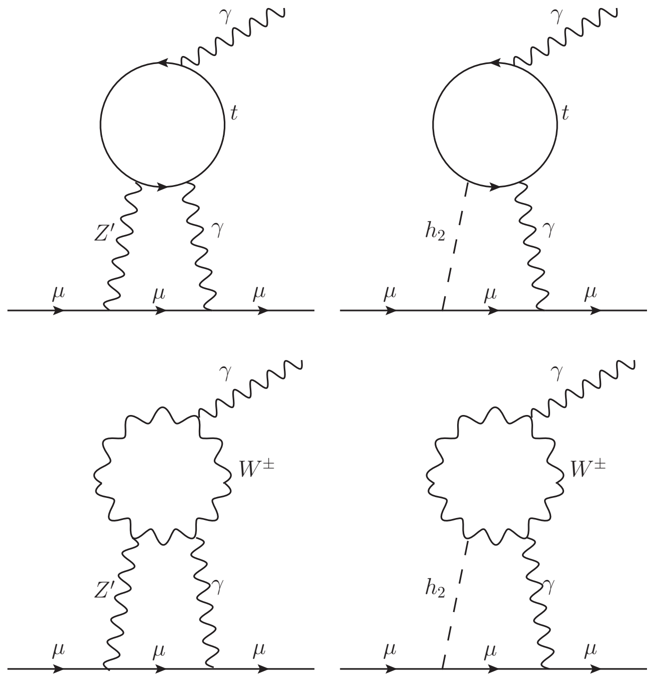

Figure 3.7: Barr-Zee type two-loop diagrams contributing to Δa_μ.

as we show in Eq. (6.14), it gets simplified to

$$\mathrm{T}_7\left(m_{Z'}^2, m_t^2, m_t^2\right) \simeq \frac{2}{m_{Z'}^2}\,, \tag{3.43}$$

up to a small truncation error (see Appendix 6.1 for details). For the parameter space region under consideration the difference $g_{\mathrm{L}}^{ttZ'} - g_{\mathrm{R}}^{ttZ'}$ can be cast in a simplified form as follows

$$\left(g_{\mathrm{L}}^{ttZ'} - g_{\mathrm{R}}^{ttZ'}\right) \simeq \frac{(g^2 + g_{\mathrm{Y}}^2)\, g_{\mathrm{YB}}}{32 g_{\mathrm{B\text{-}L}}} \left(\frac{v}{x}\right)^2 . \tag{3.44}$$

Using this result and the approximate value of the loop factor, we can calculate the ratio between the two- and one-loop contributions to the muon $(g-2)_\mu$,

$$\frac{\Delta a_\mu^{\gamma Z'}}{\Delta a_\mu^{Z'}} \simeq -\frac{g^2 g_{\mathrm{Y}^2}}{2048\pi^2} \frac{g_{\mathrm{YB}}}{g_{\mathrm{B\text{-}L}}} \left(\frac{v}{x}\right)^2 \ll 1\,, \tag{3.45}$$

which shows that $\Delta a_\mu^{\gamma Z'}$ does indeed play a subdominant role in our analysis and can be safely neglected.

3.3 The B-L-SM Conclusions

In this chapter, we have confronted the model with the most recent experimental bounds from the direct Z' boson and next-to-lightest Higgs state searches at the LHC. Simultaneously, we have analysed the prospects of the B-L-SM for a consistent explanation of the observed anomaly in the muon anomalous magnetic moment $(g-2)_\mu$. Done through exploring B-L-SM potential for the observed $(g-2)_\mu$ anomaly in the regions of the model parameter space that are consistent with direct searches and electroweak precision observables.

As one of the main results of our analysis, we have found phenomenologically consistent model parameter space regions that simultaneously fit the exclusion limits from direct Z' searches and can explain the muon $(g-2)_\mu$ anomaly. We have distinguished four benchmark points for future phenomenological exploration at experiments, the first one with the lightest allowed Z' ($m_{Z'} > 3.1$ TeV), the second with the lightest additional scalar boson ($m_{h_2} > 400$ GeV), and the other two points that reproduce the muon $(g-2)_\mu$ anomaly within 1σ uncertainty range. Besides, we have studied the correlations of the Z' production cross section times the branching ratio into a pair of light leptons versus the physical parameters of the model. In particular, we have found that the muon $(g-2)_\mu$ observable dominated by Z' loop contributions lies within the phenomenologically viable parameter space domain. For completeness, we have also estimated the dominant contribution from the Barr-Zee type two-loop corrections and found a relatively small effect.

Chapter 4

Proper 3HDM

As referenced, one of the simplest ways to expand the SM is to add elements to it's scalar sectors, on the previous example a complex scalar field originated a additional neutral scalar in harmony with a new gauge boson. Now we will move on to another sort of BSM scenario, a three Higgs Doublet Model (3HDM). This model contains in parallel with the standard SM Higgs doublet two additional replicas of that same doublet, together these form a sort of family in the scalar sector, creating a family of scalars in analogy to the fermion sector. This idea is far from original and was first discussed by Weinberg in, [56]. Naturally all these Higgs doublets will take a VEV value in the same shape as the SM. The additional Higgs doublet would not alter the tree-level electroweak ρ parameter as long the condition that the sum of the doublet VEVs are equal the value for the electroweak VEV in case of the SM citation needed. These conditions are a natural imposition in these models.

The first model that attempted to perform a doublet based extension was the Two Higgs Doublet Model (2HDM) proposed by T.D. Lee [57]. His work motivated by the search for a spontaneous breaking of the CP symmetry. A great deal of interest was invested in 2HDMs, given their possible dark matter candidates large particle spectrum, including charged and additional neutral scalars. However, take in consideration that in most 2HDM structures the possibility of tree-level scalar mediated FCNCs emerged. A analysis of their origin led to disturbing conclusions, given the fermions now have their mass generated by several Yukawa matrices their simultaneous diagonalization wasn't guaranteed. relevant? These tree-level FCNCs are, in most cases, in direct opposition to experimental results. In fact, Consulting the literature, as in, [58], we see this forces the extra scalars to have masses above 1 TeV. These heavy scalars although a possibility given current observations, are far from ideal, since there is no indication such heavy scalars exist. There-for several mechanisms have been proposed to deal with suppress these tree-level FCNCs. First, in, [59, 60, 61], it is proposed a framework in which we have the balancing of CP-odd and CP-even contribution to FCNCs, however, this would requires some fine-tuning, making it very unappealing. Another possibility is to assume alignment between different Yukawa matrices such that no FCNCs are present, see [62, 63, 64] for more information. Finally we could also use the approach presented in the BGL (Branco-Grimus-Lavoura) version of the

2HDM [65, 66], here the authors impose a flavour-violating symmetry naturally keeping the FCNCs under control trough the CKM matrix. The phenomenology of the model has been studied quite thoroughly (see, for instance [67, 68]) and it remains a possible scenario for BSM physics. This BGL 2HDM is very relevant for our studies in this chapter, as we'll be presenting a BGL like 3HDM model based on a similar structure.

In this chapter we endeavoured to look into a next-to-minimal possibility for a BGL like 3HDM framework. We used previous work to narrow down the vast parameter space of these type of models offer, see [69, 70, 71, 72]. Our conclusions are consistent with these studies, where it was found to have large regions of parameter space which conformed with experimental constraints in the flavour and scalar sectors.

The basis for our BGL like treatment of a 3HDM will be the inclusion of a flavour symmetry, as to attempt to constrain the flavour observables. In particular the addition of a $\mathrm{U}(1) \times \mathrm{Z}_2$ symmetry. This symmetry constrains the terms that can appear in the flavour sector of the Lagrangian resulting in very specific structures (or textures) of the Yukawa couplings. We will show how this structure combined with the off diagonal terms of the CKM matrix lead to controlled values for FCNCs. Then showing that light scalars are still within the reach of future collider experiments in our model's framework while having FCNCs concurrent with observations and respecting many more theoretical and experimental bounds, such as in our previous analysis.

4.1 The formulation of a BGL-like 3HDM

Challenging the 2HDM BGL paradigm can be motivated by some phenomenological comparison of the 3HDM to the 2HDM model. For example, vacuum stability in the 2HDM model can only accommodate one instance of spontaneous CP or charge symmetry breaking [73, 74, 75]. However in Multiple Higgs Doublets models (NHDMs), such as the 3HDM, charge breaking minima were found to be stable while at the same time coexisting with charge-preserving ones, for more information see, [76]. Also, for the 2HDM a full list of all possible incorporations of symmetries consistent with $\mathrm{SU}(2)\times\mathrm{U}(1)$ has been achieved [77, 78], while for the 3HDM no work has thus far been completed, see, [70, 79]. Moreover generic unitarity constraints have been found for the 2HDM [80] but not for 3HDMs. As such, the possibility of ascertaining whether the BGL structure can be extended to a full 3HDM compels us to try to find it. Move to the top

The particle content of the model is pretty similar to the SM. Having the same gauge fields and the following fermion and scalar fields,

$$\begin{aligned} Q_{L_i} &= \begin{pmatrix} u_{L_i} \\ d_{L_i} \end{pmatrix} \quad , \quad \Psi_{L_i} = \begin{pmatrix} \nu_{L_i} \\ e_{L_i} \end{pmatrix} \quad , \\ u_{R_i} \quad &, \quad d_{R_i} \quad , \quad e_{R_i} \quad i = \{1,2,3\} \quad , \\ \phi_k &= \begin{pmatrix} W_k^{\pm} + i\, W_k^{\mp} \\ \frac{1}{\sqrt{2}}\left(v_k + h_k + iZ_k\right) \end{pmatrix} \quad , \quad k = \{1,2,3\} \quad . \end{aligned} \tag{4.1}$$

where Q_{L_i} , ϕ_k , Ψ_{L_i} and u_{R_i}, d_{R_i}, e_{R_i} are SU$(2)_L$ doublets and singlets of the i-th and k-th generation, respectively. These fields are all naturally charged under the new U$(1) \times \mathbb{Z}_2$, one can transformation these fields as,

$$\begin{array}{ll} \mathrm{U}(1): & \mathbb{Z}_2: \\ \quad Q_{L_3} \to e^{i\alpha} Q_{L_3} & \quad Q_{L_3} \to -Q_{L_3} \\ \quad u_{R_3} \to e^{2i\alpha} u_{R_3} & \quad u_{R_3} \to -u_{R_3} \\ \quad \phi_1 \to e^{i\alpha}\phi_1 & \quad \phi_1 \to -\phi_1 \\ \quad \Psi_{L_1} \to e^{i\alpha}\Psi_{L_1} & \quad \Psi_{L_1} \to -\Psi_{L_1} \\ \quad \phi_3 \to e^{i\alpha}\phi_3 & \quad \phi_3 \to -\phi_3 \end{array} \tag{4.2}$$

This symmetry will have to be softly broken as to avoid the appearance of a massless Goldstone state. All remaining fields not shown in Eq. 4.2 remain unchanged under transformations of the U$(1) \times \mathbb{Z}_2$ global symmetry.

4.1.1 Introducing The Scalar Sector

Let us then start our proper introduction to the workings of the model by presenting the scalar sector where the new spin-0 SU(2) doublets, ϕ_i, $i = \{1, 2, 3\}$ reside. Note the scalar potential to be CP-invariant, this means,

$$\phi_1 = \phi_1^* \quad , \quad \phi_2 = \phi_2^* \quad , \quad \phi_3 = \phi_3^* \tag{4.3}$$

The generic scalar potential that follows all these transformations is extensively written in,

$$\begin{aligned} V(\phi_i) = &- \mu_1^2 \left(\phi_1^\dagger \phi_1\right) - \mu_2^2 \left(\phi_2^\dagger \phi_2\right) - \mu_3^2 \left(\phi_3^\dagger \phi_3\right) \\ &\left[-\mu_{12}^2 \left(\phi_1^\dagger \phi_2\right) - \mu_{23}^2 \left(\phi_2^\dagger \phi_3\right) - \mu_{13}^2 \left(\phi_1^\dagger \phi_3\right) + h.c.\right] \\ &+ \lambda_1 \left(\phi_1^\dagger \phi_1\right) + \lambda_2 \left(\phi_2^\dagger \phi_2\right) + \lambda_3 \left(\phi_3^\dagger \phi_3\right) \\ &+ \lambda_4 \left(\phi_1^\dagger \phi_1\right)\left(\phi_2^\dagger \phi_2\right) + \lambda_5 \left(\phi_1^\dagger \phi_1\right)\left(\phi_3^\dagger \phi_3\right) + \lambda_6 \left(\phi_2^\dagger \phi_2\right)\left(\phi_3^\dagger \phi_3\right) \\ &+ \lambda_7 \left(\phi_1^\dagger \phi_2\right)\left(\phi_1^\dagger \phi_2\right) + \lambda_8 \left(\phi_1^\dagger \phi_3\right)\left(\phi_3^\dagger \phi_1\right) + \lambda_9 \left(\phi_2^\dagger \phi_3\right)\left(\phi_3^\dagger \phi_2\right) \\ &+ \lambda_{10}\left\{ \left(\phi_1^\dagger \phi_3\right)^2 + \text{h.c.}\right\} \end{aligned} \tag{4.4}$$

Recall that due to the CP symmetry imposed on this potential all parameters, $(\lambda_i, i = \{1, ..., 10\})$, here are real. The parameter μ_{23}, is necessarily added as to impede the formation of a massless axion. However the most generic version of this soft breaking is given by the second line. After the process of SBB, all Higgs doublets take a VEV shape similar to that of the SM Higgs, written as,

$$\phi_k = \begin{pmatrix} W_k^\pm + i\, W_k^\mp \\ \frac{1}{\sqrt{2}}\left(v_k + h_k + i Z_k\right) \end{pmatrix} \to \langle \phi_k \rangle = \begin{pmatrix} 0 \\ \frac{v_k}{\sqrt{2}} \end{pmatrix} \quad , \quad k = \{1, 2, 3\} \tag{4.5}$$

Here we see the charged portion of the field, $W_k^{\pm}$, the CP-odd portion, Z_k, and finally the CP-even, h_k. Where the sum of the VEVs must satisfy,

$$\sum_{k=1}^{3} v_k^2 = 246^2 \text{GeV} \quad . \tag{4.6}$$

For the given scalar potential V to have a stable vacuum it needs to satisfy *boundness from below* conditions. As before this will ensure that there is indeed an absolute minimum of energy. To solve these one must write the derivates of the potential with respect to the fields and then observe their values once the process of SBB occurs, this process yields the following equations,

$$\begin{aligned}
\frac{\partial V}{\partial \phi_1} &= \frac{1}{2} v_1 \left((2\lambda_{10} + \lambda_5 + \lambda_8) v_3 + 2 \left(\lambda_1 v_1 + \mu_1^2 \right) + (\lambda_4 + \lambda_7) \right) \\
\frac{\partial V}{\partial \phi_2} &= \frac{1}{2} v_2 \left(2 \left(\lambda_2 v_2^2 + \mu_2^2 \right) + (\lambda_4 + \lambda_7) v_1^2 + (\lambda_9 + \lambda_6) v_3^2 \right) + \mu_{23} v_3 \\
\frac{\partial V}{\partial \phi_3} &= \frac{1}{2} \left((2\lambda_{10} + \lambda_5 + \lambda_8) v_1^2 + 2\mu_3^2 + (\lambda_6 + \lambda_9) v_2^2 \right) v_3 + \lambda_3 v_3^3 + \mu_{23}^2 v_2
\end{aligned} \tag{4.7}$$

By requiring that the derivatives of the potential vanish for some value of the CP-even fields ϕ_i , one arrives at the so-called tadpole equations of the model. And trough the tadpole equations in Eq. 4.7, we could express the quadratic terms μ_1, μ_2 and μ_3 as follows,

$$\begin{aligned}
\mu_1^2 &= \lambda_1 v_1^2 + \frac{1}{2} (\lambda_4 + \lambda_7) v_2^2 + \frac{1}{2} (\lambda_5 + \lambda_8 + 2\lambda_{10}) v_2^2 \\
\mu_2^2 &= \lambda_2 v_2^2 + \frac{1}{2} (\lambda_4 + \lambda_7) v_1^2 + \frac{1}{2} (\lambda_6 + \lambda_9) v_3^2 + \frac{v_3}{v_2} \mu_{23}^2 \\
\mu_3^2 &= \lambda_3 v_3^2 + \frac{1}{2} (\lambda_6 + \lambda_9) v_2^2 + \frac{1}{2} (\lambda_5 + \lambda_8 + 2\lambda_{10}) v_1^2 + \frac{v_2}{v_3} \mu_{23}^2
\end{aligned} \tag{4.8}$$

Following these, trough Eqs. 4.8 and Eq. 4.6, we can parametrize the VEVs as a function of two mixing angles ψ_1, ψ_2 and magnitude v,

$$v_1 = v \cos(\psi_1) \cos(\psi_2) \quad , \quad v_2 = v \sin(\psi_1) \cos(\psi_2) \quad , \quad v_3 = v \sin(\psi_2) \tag{4.9}$$

where $v = \sqrt{v_1^2 + v_2^2 + v_3^2}$. Through this parametrization we can write the ortogonal matrix,

$$\mathcal{O} = \begin{pmatrix} \cos(\psi_1)\cos(\psi_2) & \cos(\psi_2)\sin(\psi_1) & \sin(\psi_2) \\ -\sin(\psi_1) & \cos(\psi_1) & 0 \\ -\cos(\psi_1)\sin(\psi_2) & \sin(\psi_1)\sin(\psi_2) & \cos(\psi_2) \end{pmatrix} \tag{4.10}$$

This matrix is going to form a fundamental part of our diagonalization of massive scalar states. It is also going to prove to be fundamental as we expect the lightest scalar Higgs in our 3HDM to serve as the observed SM higgs. Therefor, a linear combination of the unphysical CP-even scalar fields ϕ_i weighted by the three VEVs is impossed.

$$h_{SM} = \frac{1}{v} (v_1 \phi_1 + v_2 \phi_2 + v_3 \phi_3) \tag{4.11}$$

4.1.2 The CP-odd portion of the scalar sector

We can now turn our attention to the physical scalar spectrum of the model. This potential is explicitly CP invariant given all parameters are real (VEVs, couplings and quadratic masses). In fact in this model we expect to find no more sources of CP-violation than in the SM.

Pseudoscalar Eigenstates

The CP-odd portion of the scalar sector (related to the z_k degrees of freedom) contains quadratic terms after the process of SBB. These are easily extracted from the scalar potential in the form,

$$V_{\text{shifted}} \supset \begin{pmatrix} z_1 & z_2 & z_3 \end{pmatrix} \frac{M_P^2}{2} \begin{pmatrix} z_1 \\ z_2 \\ z_3 \end{pmatrix} \tag{4.12}$$

where M_P^2 is the 3×3 pseudoscalar mass matrix in a non diagonal form, i.e. in a unphysical basis. It can however be expressed in a block diagonalized trough the rotation matrix we introduced in Eq. 4.10, as,

$$B_P^2 = \mathcal{O} M_P^2 \mathcal{O}^T = \begin{pmatrix} 0 & 0 & 0 \\ 0 & (B_P^2)_{22} & (B_P^2)_{23} \\ 0 & (B_P^2)_{32} & (B_P^2)_{33} \end{pmatrix} \tag{4.13}$$

The line and column of zeroes in this matrix tells us that it has a zero eigenvalue. This eigenstate will provide a Goldstone, this is clearly the Goldstone that will become the longitudinal polarization of the Z. The remaining elements of the B_P^2 matrix are given by,

$$\begin{aligned} \left(B_P^2\right)_{22} &= \frac{v_3\left(-2v_2^3 v_3 \lambda_1 0 + v_1^2 \mu_{23}^2\right)}{v_2\left(v_1^2 + v_2^2\right)} \\ \left(B_P^2\right)_{32} = \left(B_P^2\right)_{23} &= \frac{v_1 v\left(2v_2 v_3 \lambda_{10} + \mu_{23}^2\right)}{v_2^2 + v_1^2} \\ \left(B_P^2\right)_{33} &= \frac{v^2\left(2v_1^2 v_3 \lambda_{10} - v_2 \mu_{23}^2\right)}{\left(v_2^2 + v_1^2\right) v_3} \end{aligned} \tag{4.14}$$

From the above equations we notice that, apart from the three VEVs, only two parameters, λ_{10} and μ_{23}, enter in the pseudoscalar mass eigensystem. Given this fact, we can introduce a final orthogonal matrix,

$$\mathcal{O}_{\gamma_1} = \begin{pmatrix} 1 & 0 & 0 \\ 0 & \cos(\gamma_1) & -\sin(\gamma_) \\ 0 & \sin(\gamma_1) & \cos(\gamma_1) \end{pmatrix} \tag{4.15}$$

Making the mass eigenstates in the mass basis to be,

$$\mathcal{O}_{\gamma_1} (B_P)^2 \mathcal{O}_{\gamma_1}^T = \begin{pmatrix} 0 & 0 & 0 \\ 0 & M_{A_1} & 0 \\ 0 & 0 & M_{A_2} \end{pmatrix} \tag{4.16}$$

Here we have the final massive states, A_1 and A_2. Furthermore, through the conditions,

$$\begin{gathered} \mathrm{Tr}(B_C^2) = m_{A_1} + m_{A_2} \\ \mathrm{Det}(B_P^2) = m_{A_1} m_{A_2} \end{gathered} \tag{4.17}$$

We can express the mass of these pseudoscalars as a paramatrization of, $\lambda_1 0$, v, and mixing angles ψ_1 and ψ_2.

$$\begin{aligned} m_{A_1} &= -2\lambda_{10} v^2 \left(1 - \sin(\psi_1)^2 \cos(\psi_2)^2\right) \\ m_{A_2} &= \frac{\mu_2 3}{\sin(\psi_1)\sin(\psi_2)\cos(\psi_2)} \left(1 - \cos(\psi_1)^2 \cos(\psi_2)^2\right) \end{aligned} \tag{4.18}$$

Charged Scalar Eigenstates

Through a similar process, we can endeavour to isolate the quadratic terms relating to the charged degrees of freedom. These fields produce a similar structure to the mass matrix of the pseudoscalar fields.

$$B_C^2 = \mathcal{O} M_C^2 \mathcal{O}^T = \begin{pmatrix} 0 & 0 & 0 \\ 0 & (B_C^2)_{22} & (B_C^2)_{23} \\ 0 & (B_C^2)_{32} & (B_C^2)_{33} \end{pmatrix} \tag{4.19}$$

Here we observe again that a line and column of zeros ensures that we have a Goldstone boson for the $W^{\pm}$. In the same fashion as before we define the terms of Eq.4.19,

$$\begin{aligned} \left(B_C^2\right)_{22} &= -\frac{1}{2v_2(v_1^2+v_2^2)} \Big[v_2^5 \lambda_7 + v_2^3 \left(2v_1^2\lambda_7 + v_3^2 \left(2\lambda_{10} + \lambda_8\right)\right) \\ &\qquad\qquad + v_2 \left(v_1^4 \lambda_7 + v_1^2 v_3^2 \lambda_9\right) - 2v_1^2 v_3 \mu_{23}^2 \Big] \\ \left(B_C^2\right)_{32} &= \frac{v_1 v}{2(v_1^2+v_2^2)} \left[v_2 v_3 \left(2\lambda_{10} + \lambda_8 - \lambda_9\right) + 2\mu_{23}^2 \right] \\ \left(B_C^2\right)_{33} &= \frac{v^2}{2(v_1^2+v_2^2)v_3} \left[v_1^2 v_3 \left(2\lambda_{10} + \lambda_8\right) + v_2 \left(v_2 v_3 \lambda_9 - 2\mu_{23}^2\right) \right] \end{aligned} \tag{4.20}$$

Again we need to introduce another base changing rotation matrix. This is,

$$\mathcal{O}_{\gamma_2} = \begin{pmatrix} 1 & 0 & 0 \\ 0 & \cos(\gamma_2) & -\sin(\gamma_2) \\ 0 & \sin(\gamma_2) & \cos(\gamma_2) \end{pmatrix} \tag{4.21}$$

Making the mass eigenstates in the mass basis to be,

$$\mathcal{O}_{\gamma_1}\left(B_C\right)^2\mathcal{O}_{\gamma_1}^T = \begin{pmatrix} 0 & 0 & 0 \\ 0 & M_{H_1^\pm} & 0 \\ 0 & 0 & M_{H_2^\pm} \end{pmatrix} \tag{4.22}$$

Where we see the explicit mass eigenstates of the charged scalars $H_1^\pm$ and $H_2^\pm$. Trough these matrices we can arrive at another parametrization,

$$\begin{aligned} m_{H_1^\pm}\cos^2(\gamma_2) + m_{H_2^\pm}\sin^2(\gamma_2) &= \left(B_C^2\right)_{22} \\ \cos(\gamma_2)\sin(\gamma_2)(m^2_{H_2^\pm} - m^2_{H_1^\pm}) &= \left(B_C^2\right)_{23} \\ m_{H_1^\pm}\sin^2(\gamma_2) + m_{H_2^\pm}\cos^2(\gamma_2) &= \left(B_C^2\right)_{33} \end{aligned} \tag{4.23}$$

Here, another three parameters of the potential can be expressed in terms of physical masses and a mixing angle.

$$\begin{aligned} \lambda_7 &= \\ \lambda_8 &= \\ \lambda_9 &= \end{aligned} \tag{4.24}$$

4.1.3 The CP-even portion of the scalar sector

Following the same procedure as we did for the CP-odd portion we begin by approaching the quadratic portion of the scalar fields in the potential,

$$V \supset \begin{pmatrix} h_1 & h_2 & h_3 \end{pmatrix} \frac{M_S^2}{2} \begin{pmatrix} h_1 \\ h_2 \\ h_3 \end{pmatrix} \tag{4.25}$$

where M_S^2 is a 3×3 symmetric matrix. The elements of this matrix are given by,

$$M_S^2 = \begin{pmatrix} 2v_1^2\lambda_1 & v_1v_2\left(\lambda_4+\lambda_7\right) & v_1v_3\left(\lambda_{10}+\lambda_5+\lambda_8\right) \\ 0 & 2v_2^2\lambda_2 + \frac{v_3\mu_{23}^2}{v_2} & v_2v_3\left(\lambda_6+\lambda_9\right) - \mu_{23}^2 \\ 0 & 0 & 2v_3^2\lambda_3 + \frac{v_2\mu_{23}^2}{v_3} \end{pmatrix} \tag{4.26}$$

This matrix has to be diagonalized to reach the massive eigenstates. Moving to the mass basis, h, H_1 and H_2 we use,

$$\begin{pmatrix} h \\ H_1 \\ H_2 \end{pmatrix} = \mathcal{O}_\alpha \begin{pmatrix} h_1 \\ h_2 \\ h_3 \end{pmatrix} \tag{4.27}$$

Here $\mathcal{O}_\alpha$ can be parametrized as,

$$\mathcal{O}_\alpha = R_1\cdot R_2\cdot R_3 \quad , \tag{4.28}$$

with,

$$R_1 = \begin{pmatrix} \cos(\alpha_1) & \sin(\alpha_1) & 0 \\ -\sin(\alpha_1) & \cos(\alpha_1) & 0 \\ 0 & 0 & 1 \end{pmatrix} \quad , \quad R_2 = \begin{pmatrix} \cos(\alpha_2) & 0 & \sin(\alpha_2) \\ 0 & 1 & 0 \\ -\sin(\alpha_2) & 0 & \cos(\alpha_2) \end{pmatrix} \quad , \tag{4.29}$$

(4.30)

$$R_3 = \begin{pmatrix} 1 & 0 & 0 \\ 0 & \cos(\alpha_3) & \sin(\alpha_3) \\ 0 & -\sin(\alpha_3) & \cos(\alpha_3) \end{pmatrix} \quad . \tag{4.31}$$

Through this $\mathcal{O}_\alpha$ we can diagonalize scalar massive eigenstates.

$$\mathcal{O}_\alpha M_S^2 \mathcal{O}_\alpha^T \equiv \mathrm{diag}(m_h, m_{H_1}, m_{H_2}) \tag{4.32}$$

Here we can perform another inversion, allowing us to reach a parametrization of the six remaining couplings,

$$\begin{gathered} \lambda_1 \\ \lambda_2 \\ \lambda_3 \\ \lambda_4 \\ \lambda_5 \\ \lambda_6 \end{gathered} \tag{4.33}$$

To recapitulate, we can express the original fourteen real parameters of the potential in terms of physical constants. First using tadpole equations to reach μ_{21} , μ_{22} and μ_{23} in relation to the three VEVs. Secondly μ_{23} and $\lambda_1 0$, can be exchanged for m_{A_1} and m_{A_2}. Finally the remaining nine quartic couplings five physical masses (three CP-even scalars, and two charged scalars) and three mixing angles (three in the CP-even sector and one in the charged scalar sector).

In all these relations will impose the strict alignment limit condition. This translates in the lightest scalar state m_h equal to 125.09 GeV, thus making α_1 and α_2 equal to ψ_1 and ψ_2. This forces all interactions of the lightest scalar h_1 to be exactly like that of the SM, ensure it's interactions with the W and Z boson remain the same i.e. the h_1 field completely overlaps with h and H_1 and H_2 are a ortogonal mix of the fields h_2 and h_3.

4.2 Introducing the Yukawa sector

Moving onto the Yukawa portion of the Model, we can write the Yukawa sector to be,

$$\begin{aligned} \mathcal{L}_Y = & -\sum_{k=1}^{3} \left[\overline{Q}_{L_a} (\Gamma_k)_{ab} \sigma_k n_{R_b} + \overline{Q}_{L_a} (\Delta_k)_{ab} \tilde{\phi}_k p_{R_b} + h.c. \right] \\ & + (\Psi_{L_a} (Y_1^e)_{ab} \phi_1 e_{R_b} + \mathrm{h.c}) \end{aligned} \tag{4.34}$$

Here we see the quark and lepton interactions, note that Γ_k and Δ_k are the down and up Yukawa matrices in the 3HDM model respectively, one for each k generation. Notice how the leptons couple only to the first generation Higgs Doublet The lepton Yukawa matrix is assumed to be diagonal as in the SM, allowing leptons to couple exclusively to the lightest doublet, ϕ_1. Making the Yukawa matrix for Leptons to be,

$$Y_1^e = \frac{\sqrt{2}}{v_1} M_{\text{diag.}}\,(m_e, m_\mu, m_\tau) \tag{4.35}$$

However, examining the effects the imposed symmetry, $\mathrm{U}(1)\times\mathbb{Z}_2$, had on the at the shape of the yukawa matrices leads us to discover they have a very peculiar structure, their texture.

$$\begin{aligned}
\Gamma_1 &= \begin{pmatrix} 0 & 0 & 0 \\ 0 & 0 & 0 \\ \times & \times & 0 \end{pmatrix} \quad , \quad \Delta_1 = \begin{pmatrix} 0 & 0 & 0 \\ 0 & 0 & 0 \\ 0 & 0 & 0 \end{pmatrix} \quad , \\
\Gamma_2 &= \begin{pmatrix} \times & \times & 0 \\ \times & \times & 0 \\ 0 & 0 & 0 \end{pmatrix} \quad , \quad \Delta_2 = \begin{pmatrix} \times & \times & 0 \\ \times & \times & 0 \\ 0 & 0 & 0 \end{pmatrix} \quad , \\
\Gamma_3 &= \begin{pmatrix} 0 & 0 & 0 \\ 0 & 0 & 0 \\ 0 & 0 & \times \end{pmatrix} \quad , \quad \Delta_3 = \begin{pmatrix} 0 & 0 & 0 \\ 0 & 0 & 0 \\ 0 & 0 & \times \end{pmatrix} \quad .
\end{aligned} \tag{4.36}$$

Note, here the $\times$ represent a complex non-zero value in the respective matrix. We can immediately see the treatment of the first generation of quarks differ, but more than that, these textures of the Yukawa matrices and the size of their components will determine the strength of FCNCs at tree and loop-levels. You can see these Yukawa Matrices include FCNCs at tree level given their non diagonal entries, these FCNCs are suppressed by the CKM matrix.

The quadratic terms that spawn in the Lagrangian after SBB have the following relations to the Yukawa matrices,

$$\begin{aligned}
M_n &= \frac{v_1}{\sqrt{2}}\Gamma_1 + \frac{v_2}{\sqrt{2}}\Gamma_2 + \frac{v_3}{\sqrt{2}}\Gamma_3 \quad , \\
M_p &= \frac{v_1}{\sqrt{2}}\Delta_1 + \frac{v_2}{\sqrt{2}}\Delta_2 + \frac{v_3}{\sqrt{2}}\Delta_3 \quad .
\end{aligned} \tag{4.37}$$

Here we see for the first time the origin of the tree-level FCNCs. Given the Yukawa textures the mass diagonalization of the Yukawa sector is not possible. We observe the following mass matrices,

$$m_n = \begin{pmatrix} \times & \times & 0 \\ \times & \times & 0 \\ 0 & 0 & \times \end{pmatrix} \quad m_p = \begin{pmatrix} \times & \times & 0 \\ \times & \times & 0 \\ \times & \times & \times \end{pmatrix} \tag{4.38}$$

We must be able to transform the unphysical n and p into their proper quark fields d and u respectively This, like in the SM, is achieved by a set of bi-unitarity transformations, $V_{L,R}$ and $U_{L,R}$. Where naturally the CKM matrix will be $V_{\text{CKM}} = V_L^\dagger U_R$. These matrices are defined such,

$$\begin{aligned} m^d_{\text{diag}} &= U^n_L M_n U^n_R \approx U^n_L \begin{pmatrix} \times & \times & 0 \\ \times & \times & 0 \\ 0 & 0 & \times \end{pmatrix} U^n_R \\ m^u_{\text{diag}} &= U^p_L M_p U^p_R \approx U^p_L \begin{pmatrix} \times & \times & 0 \\ \times & \times & 0 \\ \times & \times & \times \end{pmatrix} U^p_R \end{aligned} \tag{4.39}$$

This then imposes certain shapes to the unitary transformations we apply,

$$\begin{aligned} V^p_L = \begin{pmatrix} \times & \times & 0 \\ \times & \times & 0 \\ 0 & 0 & 1 \end{pmatrix} \quad V^p_R &= \begin{pmatrix} \times & \times & 0 \\ \times & \times & 0 \\ 0 & 0 & e^{i\alpha} \end{pmatrix} \\ U^n_{L,R} = \begin{pmatrix} \times & \times & \times \\ \times & \times & \times \\ \times & \times & \times \end{pmatrix} \end{aligned} \tag{4.40}$$

We introduce a complex phase in U^p so that these matrices can be parametrized with two angles. While the parametrization of U^n will require 3. We know these to be the physical degrees of freedom that will be included in the CKM matrix. The CKM matrix is deduced from,

$$V_{CKM} = V^p_L U^{n\,\dagger}_R$$

$$\begin{pmatrix} V_{ud} & V_{us} & V_{ub} \\ V_{cd} & V_{cs} & V_{cb} \\ V_{td} & V_{ts} & V_{tb} \end{pmatrix} = \begin{pmatrix} V^p_{L,11} & V^p_{L,12} & 0 \\ V^p_{L,21} & V^p_{L,22} & 0 \\ 0 & 0 & e^{i\alpha} \end{pmatrix} \begin{pmatrix} U^n_{R,11} & U^n_{R,12} & U^n_{R,13} \\ U^n_{R,21} & U^n_{R,22} & U^n_{R,23} \\ U^n_{R,31} & U^n_{R,32} & U^n_{R,33} \end{pmatrix}^\dagger \tag{4.41}$$

4.3 The BGL-like suppression of FCNCs in the 3HDM model

Let us now analyse carefully the Yukawa couplings between the neutral scalar eigenstates and the physical quarks, with particular attention to any FCNC couplings which may arise.

For a first approximation to the FCNC couplings, let us define the following intermediate basis for the CP-even scalars

4.4 Numerical Results

4.4.1 Methodology

The methodology used in this numerical analysis is the same as introduced in the B-L-SM section. However with one new addition, the use of the python3 package called flavio. SPheno can be made to calculate all Wilson coefficients and these can be fed into flavio as to calculate FCNC values for our points.

4.4.2 Constraints

For any BSM theory we must ensure it can be as accurate at least as the SM in describing particle interactions. For multiscalar models such as the 3HDM, there is a wealth of bounds that are imposed upon the model's parameters so that it complies with constraints both theoretical and experimental bounds.

Given the large scalar content of the 3HDM special attention needs to be focussed on the possibility of the scalar potential becoming unbounded-from-below. Some necessary conditions are easy to find, looking at Eq. 4.4, such as the following couplings being positive so that the potential does not tend towards $-\inf$ when the fields become large.

$$\lambda_1 > 0 \quad , \quad \lambda_2 > 0 \quad , \quad \lambda_3 > 0 \quad , \tag{4.42}$$

To further find the proper conditions we must follow a procedure similar to the one used in the 2HDM [65]. By taking two doublets at a time (i, j) to infinity but such that ensuring that $\phi_i^\dagger \phi_j = 0$ (which is easily accomplish-able, if for one doublet the upper components are zero and for the other one the lower components vanish) one obtains a positive value of the potential for any value of the fields if,

$$\lambda_4 > -2\sqrt{\lambda_1\lambda_2} \quad , \quad \lambda_5 > -2\sqrt{\lambda_1\lambda_3} \quad , \quad \lambda_6 > -2\sqrt{\lambda_2\lambda_3} \tag{4.43}$$

We can also adapt the bounded-from-below necessary conditions from ref. [81] (their expressions 21–24), being careful with the fact that the potential of that work is different from ours (ours has a more restrictive symmetry, and therefore less quartic couplings). This translates into a generalisation of the above conditions, which become

$$\lambda_4 > -2\sqrt{\lambda_1\lambda_2} - \min(0,\lambda_7) \quad , \quad \lambda_5 > -2\sqrt{\lambda_1\lambda_3} - \min(0,\lambda_8 - 2\|\lambda_{10}\|) \\ \lambda_6 > -2\sqrt{\lambda_2\lambda_3} - \min(0,\lambda_9) \quad . \tag{4.44}$$

These conditions eliminate a great deal of parameter space, and though they are not sufficient ones, they should cover most of the parameter space leading to an unbounded-from-below potential. Other bounds are applied in the potential, such as the upper perturbatively bound, ensuring all couplings are maintained bellow 4π and Unitarity. In the SM there is a upper bound on the mass Higgs boson [82, 83], and similar processes were made for the 2HDM in [80] however no such generalization has been attempted for the 3HDM.

To constrain the unitarity, one must calculate the scattering amplitudes of scalar to scalar processes, useally denoted as a_0, and impose a upper bound on a_0 such that $\|a_0\| < \frac{1}{2}$. In multiple scalar models a so called S-matrix, comprised of all these amplitudes, has to be diagonalized, we leave this calculation for such a large system to SPheno.

Finally, a "standard" constraint on multiscalar models is to verify their compliance with electroweak precision bounds. Models with N Higgs doublets automatically satisfy $\rho = 1$ at tree-level, meaning bounds on the oblique parameter S will be easily satisfied – but that is no longer true for the T parameter, which must be computed for each model considered citation ?. These parameters are also calculated by SPheno.

Higgs constraints

Since the discovery of the Higgs boson in 2012 the LHC collaborations have been able to verify that its properties conform by and large to those expected for the SM Higgs. This means, in practical terms, that the couplings of the 125 GeV h state to electroweak gauge bosons and fermions in a BSM model cannot deviate too much from the corresponding SM couplings. A convenient way of parametrizing this is by introducing the κ-formalism, defining the dimensionless quantities.

$$\kappa_X^2 = \frac{\Gamma^{\text{BSM}}(h \to X)}{\Gamma^{\text{SM}}(h \to X)} \tag{4.45}$$

through the decay amplitudes Γ, computed in some BSM model and in the SM, of the Higgs to a certain final state X (typically ZZ, WW , $\tau\overline{\tau}$ and bb). This definition means that exact SM behaviour would correspond to $\kappa = 1$, and LHC measurements [84, 85], already only allow a roughly 20% deviation from unity for the several $\kappa's$.

4.4.3 Scalar Sector

4.4.4 Flavour

4.4.5 Fine Tuning

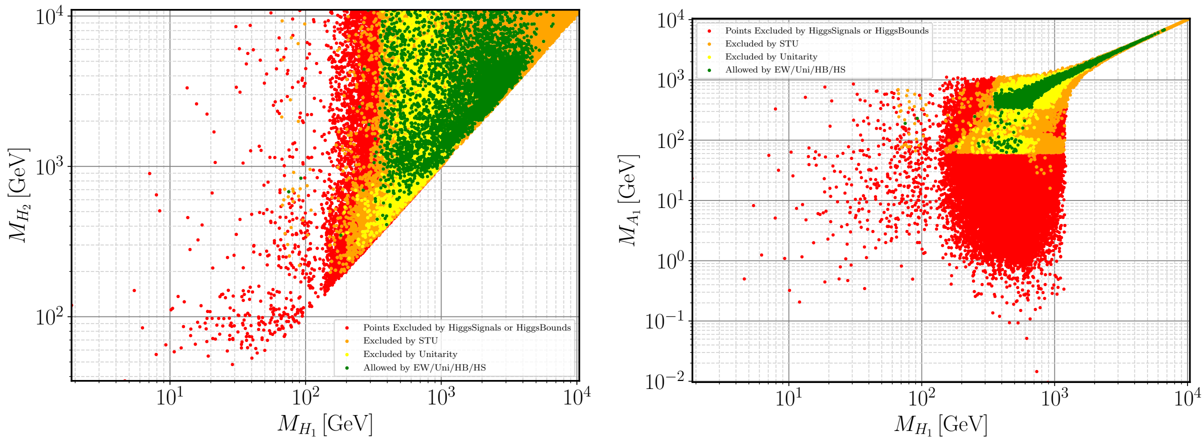

Figure 4.1: Scatter plots of parameter space allowed under several cuts imposed on the BGL-like 3HDM. Right we have the plot showing the masses of the two heavier CP-even scalars H_2 and H_1 while in the right we show the relation between the lightest (non-h) of the CP-even and pseudoscalar particles. Red points failed HS and HB tests; yellow points violate unitarity constraints; orange points only fail electroweak precision constraints, and green ones satisfy all restrictions.

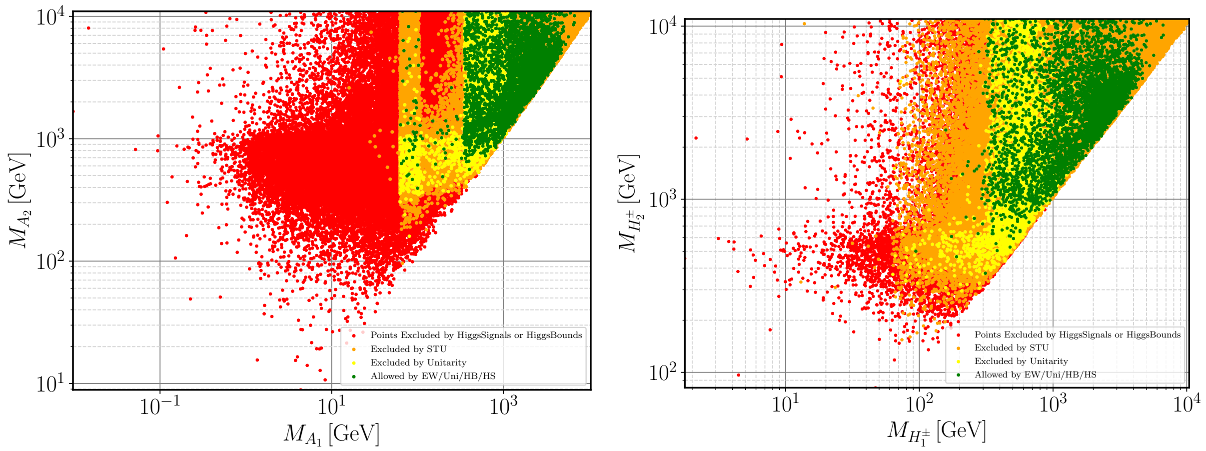

Figure 4.2:

O

4.4.6 Flavour results

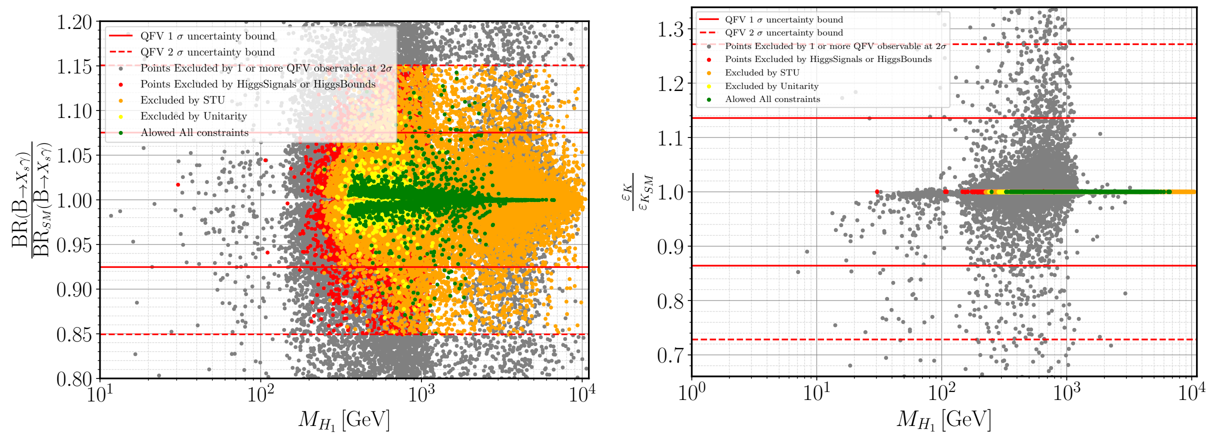

Figure 4.3: Scatter plots of parameter space allowed under several cuts imposed on the BGL-like 3HDM. Right we have the plot showing the masses of the two heavier CP-even scalars H_2 and H_1 while in the right we show the relation between the lightest (non-h) of the CP-even and pseudoscalar particles. Red points failed HS and HB tests; yellow points violate unitarity constraints; orange points only fail electroweak precision constraints, and green ones satisfy all restrictions.

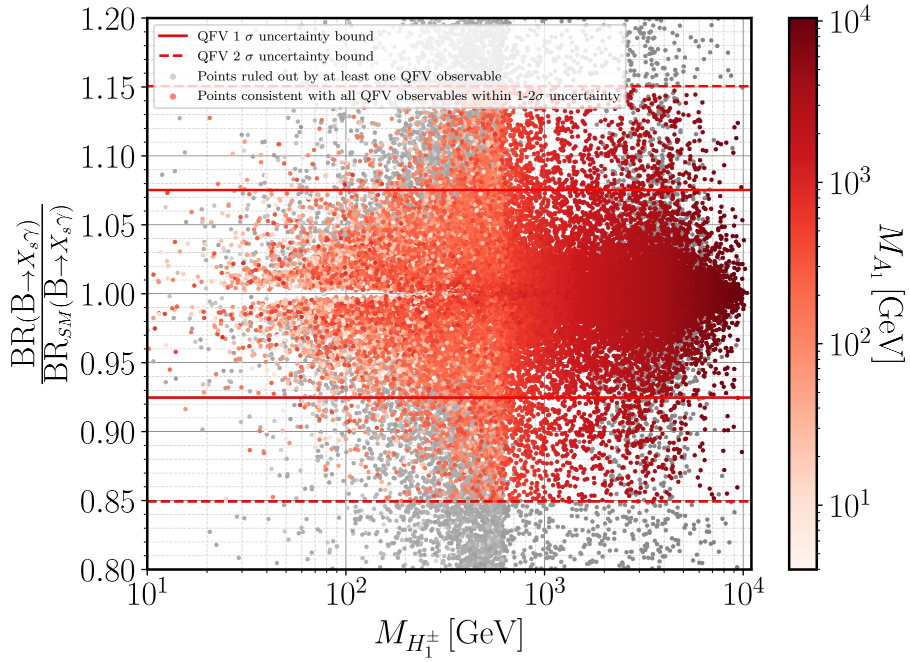

Figure 4.4:

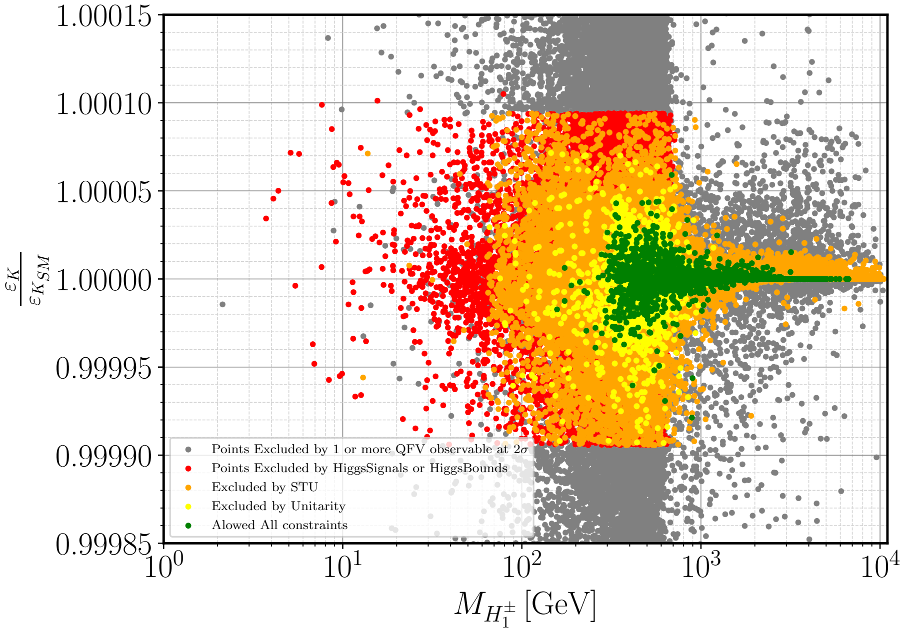

Figure 4.5:

Fine-Tuning

4.4.7 Conclusions

New scalars with masses below the TeV scale can still successfully negotiate the constraints arising from flavour data.

4.5 Old

We have studied the main features and the phenomenological consistency of a family non-universal Three Higgs Doublet Model or 3HDM with a softly broken $\mathrm{U}(1) \times \mathrm{Z}_2$ symmetry group. This broken symmetry will justify the flavour hierarchies in the SM and trough a Branco-Grimus-Lavoura mechanism supress the otherwise expected Flavour Changing Neutral Currents.

Let us now consider an extended version of the SM, with an enlarged Higgs sector that contains three generations of scalar-doublets. These Higgs will be named ϕ^i with $i = 1, 2, 3$. In this sector we must enforce the alignment limit to the scalar sector ensuring the physical scalar spectrum accommodates a SM-like Higgs boson with mass of 125.09 GeV.

Chapter 5

Future Work

Chapter 6

Appendix

6.0.1 Gamma Matrices

The γ matrices are defined as,

$$\{\gamma^\mu, \gamma^\nu\} = 2g^{\mu\nu} I \tag{6.1}$$

where,

$$g^{\mu\nu} = \begin{pmatrix} 1 & 0 & 0 & 0 \\ 0 & -1 & 0 & 0 \\ 0 & 0 & -1 & 0 \\ 0 & 0 & 0 & -1 \end{pmatrix} \tag{6.2}$$

and if $\gamma_\mu = (\gamma^0, \gamma)$ then it is usual to require for the hermitian conjugate matrices,

$$\gamma^{0\dagger} = \gamma^0 \quad \text{and} \quad \gamma^\dagger = -\gamma \tag{6.3}$$

6.0.2 Lagrangian Dynamics

In Lagrangian dynamics we define the action S has,

$$\mathcal{S} = \int L\, dt = \int \mathcal{L}(\phi, \partial\phi)\, d^4x \tag{6.4}$$

where L is the Lagrangian, and the $\mathcal{L}$ is designated as the *Lagrangian density*, note these terms are usually used interchangeable. Here $\mathcal{L}$ is a function of the field ϕ and it's spatial derivatives.

The action S is constrained by the principle of least action, this requires the "path" taken by a field between an initial and final set of coordinates to leave the action invariant, this can be expressed by,

$$\partial\mathcal{S} = 0 \tag{6.5}$$

from here one can deduce the *Euler-Lagrange* equations,

$$\partial_\mu \left(\frac{\partial \mathcal{L}(\phi, \partial\phi)}{\partial(\partial_\mu)} \right) - \frac{\partial \mathcal{L}(\phi, \partial\phi)}{\partial\phi} = 0 \tag{6.6}$$

6.1 The loop integral $\mathrm{T}_7(x, y, x)$

In Appendix B of Ref. [55], the exact integral equations for $\mathrm{T}_7(x, y, z)$ are provided. In our analysis we consider the limit where $x \gg y = z$, with $x = m_{Z'}^2$ and $y = z = m_t^2$, where Eq. (3.43) provides a good approximation up to a truncation error. Here, we show the main steps in determining Eq. (3.43). The exact form of the loop integral reads as

$$\begin{aligned} \mathrm{T}_7(x, y, y) = &- \frac{1}{x^2}\varphi_0(y, y) + 2y\frac{\partial^3\Phi(x, y, y)}{\partial x \partial y^2} + \frac{\partial^2\Phi(x, y, y)}{\partial x^2} + x\frac{\partial^3\Phi(x, y, y)}{\partial x^2 \partial y} \\ &+ \frac{\Phi(x, y, y)}{x^2} - \frac{1}{x}\frac{\partial\Phi(x, y, y)}{\partial x} + \frac{\partial^2\Phi(x, y, y)}{\partial x \partial y}, \end{aligned} \tag{6.7}$$

with $\varphi_0(x, y)$ and $\Phi(x, y, z)$ defined in Ref. [55]. Let us now expand each of the terms for $x \ll y$. While the first term is exact and has the form

$$-\frac{1}{x^2}\varphi_0(y, y) = -2\frac{y}{x^2}\log^2 y\,, \tag{6.8}$$

the second can be approximated to

$$2y\frac{\partial^3\Phi(x, y, y)}{\partial x \partial y^2} \simeq \xi\frac{24}{x} = \frac{8}{x} \text{ for } \xi = \frac{1}{3}\,. \tag{6.9}$$

In Eq. (6.9), the $\xi = \frac{1}{3}$ factor was introduced in order to compensate for a truncation error. This was obtained by comparing the numerical values of the exact expression and our approximation. The third term can be simplified to

$$\frac{\partial^2\Phi(x, y, y)}{\partial x^2} \simeq \frac{2}{x}\left(\log y - \log\frac{y}{x}\right) + \frac{2}{x}\,, \tag{6.10}$$

and the fourth to

$$x\frac{\partial^3\Phi(x, y, y)}{\partial x^2 \partial y} \simeq -\frac{4}{x}\left(\log\frac{y}{x} + 1\right)\,. \tag{6.11}$$

The fifth and the seventh terms read

$$\frac{\Phi(x, y, y)}{x^2} - \frac{1}{x}\frac{\partial\Phi(x, y, y)}{\partial x} \simeq \frac{2}{x}\log\frac{1}{x}\,, \tag{6.12}$$

and finally, the sixth terms can be expanded as

$$\frac{\partial^2\Phi(x, y, y)}{\partial x \partial y} \simeq \frac{4}{x}\left(\log\frac{y}{x} - 1\right)\,. \tag{6.13}$$

Noting that Eq. (6.8) is of the order $\frac{1}{x^2}$, putting together Eqs. (6.7), (6.9), (6.10), (6.11), (6.12), and (6.13) we get for the leading $\frac{1}{x}$ contributions the following:

$$\mathrm{T}_7\left(x,y,y\right) \simeq \overbrace{\frac{2}{x}\left(\log y - \log\frac{y}{x}\right) + \frac{2}{x}\log\frac{1}{x}}^{0}\overbrace{-\frac{4}{x}\left(\log\frac{y}{x}+1\right) + \frac{4}{x}\left(\log\frac{y}{x}-1\right)}^{-\frac{8}{x}} + \frac{8}{x} + \frac{2}{x} \simeq \frac{2}{x}\,. \tag{6.14}$$

Bibliography

[1] M. Aaboud *et al.*, "Search for new high-mass phenomena in the dilepton final state using 36 fb^{-1} of proton-proton collision data at $\sqrt{s} = 13$ TeV with the ATLAS detector," *JHEP*, vol. 10, p. 182, 2017.

[2] G. Aad, T. Abajyan, B. Abbott, J. Abdallah, S. Abdel Khalek, A. Abdelalim, O. Abdinov, R. Aben, B. Abi, M. Abolins, and et al., "Observation of a new particle in the search for the standard model higgs boson with the atlas detector at the lhc," *Physics Letters B*, vol. 716, p. 1–29, Sep 2012.

[3] S. Chatrchyan, V. Khachatryan, A. M. Sirunyan, A. Tumasyan, W. Adam, E. Aguilo, T. Bergauer, M. Dragicevic, J. Er, C. Fabjan, *et al.*, "Observation of a new boson at a mass of 125 gev with the cms experiment at the lhc," *Physics Letters B*, vol. 716, no. 1, pp. 30–61, 2012.

[4] C. Collaborations *et al.*, "Combined measurement of the higgs boson mass in pp collisions at sqrt s = 7 and 8 tev with the atlas and cms experiments," *arXiv preprint arXiv:1503.07589*, 2015.

[5] C. Collaborations *et al.*, "Measurements of the higgs boson production and decay rates and constraints on its couplings from a combined atlas and cms analysis of the lhc pp collision data at sqrt s = 7 and 8 tev," *arXiv preprint arXiv:1606.02266*, 2016.

[6] P. W. Higgs, "Broken symmetries and the masses of gauge bosons," *Physical Review Letters*, vol. 13, no. 16, p. 508, 1964.

[7] F. Englert and R. Brout, "Broken symmetry and the mass of gauge vector mesons," *Physical Review Letters*, vol. 13, no. 9, p. 321, 1964.

[8] G. Guralnik, C. Hagen, and T. Kibble, "Global conservation laws and massless particles 1964 phys," *Rev. Lett*, vol. 13, no. 585, p. 169, 1964.

[9] H. D. Politzer, "Reliable perturbative results for strong interactions?," *Physical Review Letters*, vol. 30, no. 26, p. 1346, 1973.

[10] D. J. Gross and F. Wilczek, "Ultraviolet behavior of non-abelian gauge theories," *Physical Review Letters*, vol. 30, no. 26, p. 1343, 1973.

[11] M. Tanabashi, K. Hagiwara, K. Hikasa, K. Nakamura, Y. Sumino, F. Takahashi, J. Tanaka, K. Agashe, G. Aielli, C. Amsler, M. Antonelli, D. Asner, H. Baer, S. Banerjee, R. Barnett, T. Basaglia, C. Bauer, J. Beatty, V. Belousov, J. Beringer, S. Bethke, A. Bettini, H. Bichsel, O. Biebel, K. Black, E. Blucher, O. Buchmuller, V. Burkert, M. Bychkov, R. Cahn, M. Carena, A. Ceccucci, A. Cerri, D. Chakraborty, M.-C. Chen, R. Chivukula, G. Cowan, O. Dahl, G. D'Ambrosio, T. Damour, D. de Florian, A. de Gouvêa, T. DeGrand, P. de Jong, G. Dissertori, B. Dobrescu, M. D'Onofrio, M. Doser, M. Drees, H. Dreiner, D. Dwyer, P. Eerola, S. Eidelman, J. Ellis, J. Erler, V. Ezhela, W. Fetscher, B. Fields, R. Firestone, B. Foster, A. Freitas, H. Gallagher, L. Garren, H.-J. Gerber, G. Gerbier, T. Gershon, Y. Gershtein, T. Gherghetta, A. Godizov, M. Goodman, C. Grab, A. Gritsan, C. Grojean, D. Groom, M. Grünewald, A. Gurtu, T. Gutsche, H. Haber, C. Hanhart, S. Hashimoto, Y. Hayato, K. Hayes, A. Hebecker, S. Heinemeyer, B. Heltsley, J. Hernández-Rey, J. Hisano, A. Höcker, J. Holder, A. Holtkamp, T. Hyodo, K. Irwin, K. Johnson, M. Kado, M. Karliner, U. Katz, S. Klein, E. Klempt, R. Kowalewski, F. Krauss, M. Kreps, B. Krusche, Y. Kuyanov, Y. Kwon, O. Lahav, J. Laiho, J. Lesgourgues, A. Liddle, Z. Ligeti, C.-J. Lin, C. Lippmann, T. Liss, L. Littenberg, K. Lugovsky, S. Lugovsky, A. Lusiani, Y. Makida, F. Maltoni, T. Mannel, A. Manohar, W. Marciano, A. Martin, A. Masoni, J. Matthews, U.-G. Meißner, D. Milstead, R. Mitchell, K. Mönig, P. Molaro, F. Moortgat, M. Moskovic, H. Murayama, M. Narain, P. Nason, S. Navas, M. Neubert, P. Nevski, Y. Nir, K. Olive, S. P. Griso, J. Parsons, C. Patrignani, J. Peacock, M. Pennington, S. Petcov, V. Petrov, E. Pianori, A. Piepke, A. Pomarol, A. Quadt, J. Rademacker, G. Raffelt, B. Ratcliff, P. Richardson, A. Ringwald, S. Roesler, S. Rolli, A. Romaniouk, L. Rosenberg, J. Rosner, G. Rybka, R. Ryutin, C. Sachrajda, Y. Sakai, G. Salam, S. Sarkar, F. Sauli, O. Schneider, K. Scholberg, A. Schwartz, D. Scott, V. Sharma, S. Sharpe, T. Shutt, M. Silari, T. Sjöstrand, P. Skands, T. Skwarnicki, J. Smith, G. Smoot, S. Spanier, H. Spieler, C. Spiering, A. Stahl, S. Stone, T. Sumiyoshi, M. Syphers, K. Terashi, J. Terning, U. Thoma, R. Thorne, L. Tiator, M. Titov, N. Tkachenko, N. Törnqvist, D. Tovey, G. Valencia, R. V. de Water, N. Varelas, G. Venanzoni, L. Verde, M. Vincter, P. Vogel, A. Vogt, S. Wakely, W. Walkowiak, C. Walter, D. Wands, D. Ward, M. Wascko, G. Weiglein, D. Weinberg, E. Weinberg, M. White, L. Wiencke, S. Willocq, C. Wohl, J. Womersley, C. Woody, R. Workman, W.-M. Yao, G. Zeller, O. Zenin, R.-Y. Zhu, S.-L. Zhu, F. Zimmermann, P. Zyla, J. Anderson, L. Fuller, V. Lugovsky, and P. S. and, "Review of particle physics," *Physical Review D*, vol. 98, Aug. 2018.

[12] S. L. Glashow, J. Iliopoulos, and L. Maiani, "Weak interactions with lepton-hadron symmetry," *Physical review D*, vol. 2, no. 7, p. 1285, 1970.

[13] S. Fajfer, J. F. Kamenik, and I. Nišandžić, "B$\rightarrow d * \tau\nu\tau$ sensitivity to new physics," *Physical Review D*, vol. 85, May 2012.

[14] R. N. Mohapatra and R. E. Marshak, "Local B-L Symmetry of Electroweak Interactions, Majorana Neutrinos and Neutron Oscillations," *Phys. Rev. Lett.*, vol. 44,

pp. 1316–1319, 1980. [Erratum: Phys. Rev. Lett.44,1643(1980)].

[15] L. Basso, S. Moretti, and G. M. Pruna, "Constraining the g'_1 coupling in the minimal $B - L$ Model," *J. Phys.*, vol. G39, p. 025004, 2012.

[16] L. Basso, S. Moretti, and G. M. Pruna, "Theoretical constraints on the couplings of non-exotic minimal Z' bosons," *JHEP*, vol. 08, p. 122, 2011.

[17] M. Tanabashi *et al.*, "Review of Particle Physics," *Phys. Rev.*, vol. D98, no. 3, p. 030001, 2018.

[18] G. Degrassi, S. Di Vita, J. Elias-Miro, J. R. Espinosa, G. F. Giudice, G. Isidori, and A. Strumia, "Higgs mass and vacuum stability in the Standard Model at NNLO," *JHEP*, vol. 08, p. 098, 2012.

[19] S. Alekhin, A. Djouadi, and S. Moch, "The top quark and Higgs boson masses and the stability of the electroweak vacuum," *Phys. Lett.*, vol. B716, pp. 214–219, 2012.

[20] D. Buttazzo, G. Degrassi, P. P. Giardino, G. F. Giudice, F. Sala, A. Salvio, and A. Strumia, "Investigating the near-criticality of the Higgs boson," *JHEP*, vol. 12, p. 089, 2013.

[21] M. S. Chanowitz, J. R. Ellis, and M. K. Gaillard, "The Price of Natural Flavor Conservation in Neutral Weak Interactions," *Nucl. Phys.*, vol. B128, pp. 506–536, 1977.

[22] H. Fritzsch and P. Minkowski, "Unified Interactions of Leptons and Hadrons," *Annals Phys.*, vol. 93, pp. 193–266, 1975.

[23] H. Georgi and D. V. Nanopoulos, "T Quark Mass in a Superunified Theory," *Phys. Lett.*, vol. 82B, pp. 392–394, 1979.

[24] H. Georgi and D. V. Nanopoulos, "Ordinary Predictions from Grand Principles: T Quark Mass in O(10)," *Nucl. Phys.*, vol. B155, pp. 52–74, 1979.

[25] H. Georgi and D. V. Nanopoulos, "Masses and Mixing in Unified Theories," *Nucl. Phys.*, vol. B159, pp. 16–28, 1979.

[26] Y. Achiman and B. Stech, "Quark Lepton Symmetry and Mass Scales in an E6 Unified Gauge Model," *Phys. Lett.*, vol. 77B, pp. 389–393, 1978.

[27] F. Gursey, P. Ramond, and P. Sikivie, "A Universal Gauge Theory Model Based on E6," *Phys. Lett.*, vol. 60B, pp. 177–180, 1976.

[28] F. Gursey and M. Serdaroglu, "E6 GAUGE FIELD THEORY MODEL REVISITED," *Nuovo Cim.*, vol. A65, p. 337, 1981. [,271(1981)].

[29] V. Barger, P. Langacker, M. McCaskey, M. Ramsey-Musolf, and G. Shaughnessy, "Complex Singlet Extension of the Standard Model," *Phys. Rev.*, vol. D79, p. 015018, 2009.

[30] T. Yanagida, "Horizontal gauge symmetry and masses of neutrinos," *Conf. Proc.*, vol. C7902131, pp. 95–99, 1979.

[31] M. Gell-Mann, P. Ramond, and R. Slansky, "Complex Spinors and Unified Theories," *Conf. Proc.*, vol. C790927, pp. 315–321, 1979.

[32] R. N. Mohapatra and G. Senjanovic, "Neutrino Mass and Spontaneous Parity Nonconservation," *Phys. Rev. Lett.*, vol. 44, p. 912, 1980. [,231(1979)].

[33] K. Kaneta, Z. Kang, and H.-S. Lee, "Right-handed neutrino dark matter under the $B-L$ gauge interaction," *JHEP*, vol. 02, p. 031, 2017.

[34] N. Okada and O. Seto, "Higgs portal dark matter in the minimal gauged $U(1)_{B-L}$ model," *Phys. Rev.*, vol. D82, p. 023507, 2010.

[35] S. Okada, "Z' Portal Dark Matter in the Minimal $B-L$ Model," *Adv. High Energy Phys.*, vol. 2018, p. 5340935, 2018.

[36] M. Fukugita and T. Yanagida, "Baryogenesis Without Grand Unification," *Phys. Lett.*, vol. B174, pp. 45–47, 1986.

[37] A. Pilaftsis, "CP violation and baryogenesis due to heavy Majorana neutrinos," *Phys. Rev.*, vol. D56, pp. 5431–5451, 1997.

[38] A. Pilaftsis and T. E. J. Underwood, "Resonant leptogenesis," *Nucl. Phys.*, vol. B692, pp. 303–345, 2004.

[39] S. Khalil, "TeV-scale gauged B-L symmetry with inverse seesaw mechanism," *Phys. Rev.*, vol. D82, p. 077702, 2010.

[40] F. F. Deppisch, S. Kulkarni, and W. Liu, "Searching for a light $Z\prime$ through Higgs production at the LHC," *Phys. Rev.*, vol. D100, no. 11, p. 115023, 2019.

[41] A. Czarnecki and W. J. Marciano, "The Muon anomalous magnetic moment: A Harbinger for 'new physics'," *Phys. Rev.*, vol. D64, p. 013014, 2001.

[42] S. Khalil and C. S. Un, "Muon Anomalous Magnetic Moment in SUSY B-L Model with Inverse Seesaw," *Phys. Lett.*, vol. B763, pp. 164–168, 2016.

[43] J.-L. Yang, T.-F. Feng, Y.-L. Yan, W. Li, S.-M. Zhao, and H.-B. Zhang, "Lepton-flavor violation and two loop electroweak corrections to $(g-2)_\mu$ in the B-L symmetric SSM," *Phys. Rev.*, vol. D99, no. 1, p. 015002, 2019.

[44] W. Porod, “SPheno, a program for calculating supersymmetric spectra, SUSY particle decays and SUSY particle production at e+ e- colliders,” *Comput. Phys. Commun.*, vol. 153, pp. 275–315, 2003.

[45] W. Porod and F. Staub, “SPheno 3.1: Extensions including flavour, CP-phases and models beyond the MSSM,” *Comput. Phys. Commun.*, vol. 183, pp. 2458–2469, 2012.

[46] F. Staub, “SARAH,” 2008.

[47] F. Staub, “SARAH 4 : A tool for (not only SUSY) model builders,” *Comput. Phys. Commun.*, vol. 185, pp. 1773–1790, 2014.

[48] P. Bechtle, O. Brein, S. Heinemeyer, O. Stål, T. Stefaniak, G. Weiglein, and K. E. Williams, “HiggsBounds − 4: Improved Tests of Extended Higgs Sectors against Exclusion Bounds from LEP, the Tevatron and the LHC,” *Eur. Phys. J.*, vol. C74, no. 3, p. 2693, 2014.

[49] P. Bechtle, S. Heinemeyer, O. Stål, T. Stefaniak, and G. Weiglein, “*HiggsSignals*: Confronting arbitrary Higgs sectors with measurements at the Tevatron and the LHC,” *Eur. Phys. J.*, vol. C74, no. 2, p. 2711, 2014.

[50] J. Alwall, R. Frederix, S. Frixione, V. Hirschi, F. Maltoni, O. Mattelaer, H. S. Shao, T. Stelzer, P. Torrielli, and M. Zaro, “The automated computation of tree-level and next-to-leading order differential cross sections, and their matching to parton shower simulations,” *JHEP*, vol. 07, p. 079, 2014.

[51] R. Costa, A. P. Morais, M. O. P. Sampaio, and R. Santos, “Two-loop stability of a complex singlet extended Standard Model,” *Phys. Rev.*, vol. D92, p. 025024, 2015.

[52] A. Freitas, J. Lykken, S. Kell, and S. Westhoff, “Testing the Muon g-2 Anomaly at the LHC,” *JHEP*, vol. 05, p. 145, 2014. [Erratum: JHEP09,155(2014)].

[53] S. M. Barr and A. Zee, “Electric Dipole Moment of the Electron and of the Neutron,” *Phys. Rev. Lett.*, vol. 65, pp. 21–24, 1990. [Erratum: Phys. Rev. Lett.65,2920(1990)].

[54] V. Ilisie, “New Barr-Zee contributions to $(\mathbf{g-2})$- in two-Higgs-doublet models,” *JHEP*, vol. 04, p. 077, 2015.

[55] T.-F. Feng and X.-Y. Yang, “Renormalization and two loop electroweak corrections to lepton anomalous dipole moments in the standard model and beyond (I): Heavy fermion contributions,” *Nucl. Phys.*, vol. B814, pp. 101–141, 2009.

[56] S. Weinberg, “Gauge theory ofCPNonconservation,” *Physical Review Letters*, vol. 37, pp. 657–661, Sept. 1976.

[57] T. D. Lee, “A theory of SpontaneousTViolation,” *Physical Review D*, vol. 8, pp. 1226–1239, Aug. 1973.

[58] G. C. Branco, L. Lavoura, and J. P. Silva, *CP Violation*, vol. 103. 1999.

[59] P. Ferreira, L. Lavoura, and J. P. Silva, "A soft origin for ckm-type cp violation," *Physics Letters B*, vol. 704, p. 179–188, Oct 2011.

[60] M. Nebot and J. P. Silva, "Self-cancellation of a scalar in neutral meson mixing and implications for the lhc," *Physical Review D*, vol. 92, Oct 2015.

[61] P. M. Ferreira and L. Lavoura, "No strong *cp* violation up to the one-loop level in a two-higgs-doublet model," 2019.

[62] A. Pich and P. Tuzón, "Yukawa alignment in the two-higgs-doublet model," *Physical Review D*, vol. 80, Nov 2009.

[63] M. Jung, A. Pich, and P. Tuzón, "Charged-higgs phenomenology in the aligned two-higgs-doublet model," *Journal of High Energy Physics*, vol. 2010, Nov 2010.

[64] M. Jung, A. Pich, and P. Tuzón, "$b^- \to \chi s \gamma$ rate and cp asymmetry within the aligned two-higgs-doublet model," *Physical Review D*, vol. 83, Apr 2011.

[65] G. Branco, W. Grimus, and L. Lavoura, "Relating the scalar flavour-changing neutral couplings to the ckm matrix," *Physics Letters B*, vol. 380, p. 119–126, Jul 1996.

[66] L. LAVOURA, "MODELS OF CP VIOLATION EXCLUSIVELY VIA NEUTRAL-SCALAR EXCHANGE," *International Journal of Modern Physics A*, vol. 09, pp. 1873–1888, Apr. 1994.

[67] F. J. Botella, G. C. Branco, A. Carmona, M. Nebot, L. Pedro, and M. N. Rebelo, "Physical constraints on a class of two-higgs doublet models with fcnc at tree level," *Journal of High Energy Physics*, vol. 2014, Jul 2014.

[68] F. J. Botella, G. C. Branco, M. Nebot, and M. N. Rebelo, "Flavour-changing higgs couplings in a class of two higgs doublet models," *The European Physical Journal C*, vol. 76, Mar 2016.

[69] P. Ferreira, I. P. Ivanov, E. Jiménez, R. Pasechnik, and H. Serôdio, "Cp4 miracle: shaping yukawa sector with cp symmetry of order four," *Journal of High Energy Physics*, vol. 2018, Jan 2018.

[70] I. P. Ivanov, V. Keus, and E. Vdovin, "Abelian symmetries in multi-higgs-doublet models," *Journal of Physics A: Mathematical and Theoretical*, vol. 45, p. 215201, May 2012.

[71] I. Ivanov and J. P. Silva, "Cp-conserving multi-higgs model with irremovable complex coefficients," *Physical Review D*, vol. 93, May 2016.

[72] A. Aranda, I. P. Ivanov, and E. Jiménez, "When thecincpdoes not matter: Anatomy of order-4cpeigenstates and their yukawa interactions," *Physical Review D*, vol. 95, Mar 2017.

[73] G. Branco, P. Ferreira, L. Lavoura, M. Rebelo, M. Sher, and J. P. Silva, "Theory and phenomenology of two-higgs-doublet models," *Physics Reports*, vol. 516, p. 1–102, Jul 2012.

[74] P. Ferreira, R. Santos, and A. Barroso, "Stability of the tree-level vacuum in two higgs doublet models against charge or cp spontaneous violation," *Physics Letters B*, vol. 603, p. 219–229, Dec 2004.

[75] A. Barroso, P. Ferreira, and R. Santos, "Neutral minima in two-higgs doublet models," *Physics Letters B*, vol. 652, p. 181–193, Aug 2007.

[76] A. Barroso, P. M. Ferreira, R. Santos, and J. P. Silva, "Stability of the normal vacuum in multi-higgs-doublet models," *Physical Review D*, vol. 74, Oct 2006.

[77] I. P. Ivanov, "Minkowski space structure of the higgs potential in the two-higgs-doublet model. ii. minima, symmetries, and topology," *Physical Review D*, vol. 77, Jan 2008.

[78] I. P. Ivanov, "Minkowski space structure of the higgs potential in the two-higgs-doublet model," *Physical Review D*, vol. 75, Feb. 2007.

[79] I. P. Ivanov and C. C. Nishi, "Symmetry breaking patterns in 3hdm," *Journal of High Energy Physics*, vol. 2015, Jan 2015.

[80] I. F. Ginzburg and I. P. Ivanov, "Tree-level unitarity constraints in the most general two higgs doublet model," *Physical Review D*, vol. 72, Dec 2005.

[81] S. Moretti and K. Yagyu, "Constraints on parameter space from perturbative unitarity in models with three scalar doublets," *Physical Review D*, vol. 91, Mar 2015.

[82] B. W. Lee, C. Quigg, and H. B. Thacker, "Strength of weak interactions at very high energies and the higgs boson mass," *Physical Review Letters*, vol. 38, pp. 883–885, Apr. 1977.

[83] B. W. Lee, C. Quigg, and H. B. Thacker, "Weak Interactions at Very High-Energies: The Role of the Higgs Boson Mass," *Phys. Rev.*, vol. D16, p. 1519, 1977.

[84] G. Aad, B. Abbott, J. Abdallah, O. Abdinov, B. Abeloos, R. Aben, O. S. AbouZeid, N. L. Abraham, H. Abramowicz, and et al., "Measurements of the higgs boson production and decay rates and constraints on its couplings from a combined atlas and cms analysis of the lhc pp collision data at s=7

$$\sqrt{s} = 7$$

and 8 tev," *Journal of High Energy Physics*, vol. 2016, Aug 2016.